Fabrication of Symmetric Super Capacitor Using Lithium-ion Conducting IOTA Carrageenan-Based Biopolymer Electrolytes

M. Nandhinilakshmi¹ · D. Vanitha² · N. Nallamuthu³ · K. Sundaramahalingam⁴ · P. Saranya¹

Abstract

Solid-state polymer electrolyte system that relies on an Iota carrageenan/Acacia gum blend and ethylene glycol as plasticizer incorporated with $LiNO_3$ has been synthesized using the solution cast technique. The structural characterization has done by X-ray diffraction and Fourier transform infrared (FTIR) analysis. FTIR deconvolution reveals that ion–ion interaction analysis and the free ion and contact ion percentage. The electrolyte with 30 wt% $LiNO_3$ (IAN30) has the higher conductivity as 1.77×10^{-3} S cm^{-1}, activation energy as 0.02 eV and ion transport number as 0.999. The non-Debye property of polymer electrolytes is confirmed by studies on the frequency dependence of dielectric and, dielectric loss tangent parameter β. UV spectra of IAN30 also confirms the reduction in band-gap. IAN30 is used for the fabrication of Electric double layer capacitor (EDLC) and Electrochemical cell. There are no redox peaks in the Cyclic voltammetry response through its entire potential range for EDLC behavior. From the galvanostatic charge/discharge studies of prepared symmetrical capacitor, discharge time and specific capacitance (C_s) values are calculated as 16s and 22 F/g respectively.

Keywords Iota carrageenan · Acacia gum · Lithium nitrate · AC impedance · TNM · CV · GCD, XRD, FTIR · Conduction mechanism · FTIR-deconvolution · UV

Introduction

Devices with the ability to store and release electrical energy as desired are known as electrical devices. Researchers are keener to create photovoltaic panels, sensors, super capacitors, fuel cells, and batteries as a result of the consumption for creating quality electrochemical devices. Solid biopolymer electrolytes (SBE) have experienced a drastic development in recent years [1, 2].The evolution of electrical energy storage devices took a new turn with the invention of supercapacitors. Supercapacitors are regularly employed in systems and devices that demand a high power supply due to their various benefits.

The electrode in a supercapacitor is crucial in storing a lot of charge on its surface. So, while choosing an appropriate electrode material for a super capacitor, features of the electrode including porosity, surface morphology, surface area, high specific capacitance, large scan rate capability, high cycle stability and electrical conductivity are taken into consideration. Materials that have been widely employed as electrodes include Activated carbon, CNT, Graphene, Carbon Aerogel, Metal Compounds, Conducting Polymers, and their Composites. In addition, the toxicity and cost of the active materials used in an electrode design should be taken into account as well [3, 4].

Supercapacitors use polymer electrolytes that are significantly thinner and electrodes with much greater surface areas to reduce the distance between the electrodes. This result in an increase in energy and capacitance. Electrolytes are the key for supercapacitive devices to have a high power and energy density, long cycling life, and safety. Ionic mobility and conductivity are the important factors to evaluate the performance of electrolytes.

✉ D. Vanitha
vanibala2003@gmail.com

1 Multi-Functional Materials Laboratory, International Research Center, Kalasalingam Academy of Research and Education, Virudhunagar, Tamilnadu 626126, India

2 Department of Physics, Kalasalingam Academy of Research and Education, Virudhunagar, Tamilnadu 626126, India

3 Department of Physics, Dayananda Sagar Academy of Technology and Management, Bangalore, Karnataka 560082, India

4 Department of Physics, Arulmigu Kalasalingam College of Arts and Science, Virudhunagar, Tamilnadu 626126, India

The primary goal of conducting polymer research is to create higher ionic conductivity polymer electrolytes for applications in energy storage devices. For environmental concern, biopolymers are selected and many methods are adopted to increase the conductivity. In this, Polymer blending is a method used by researchers to enhance the properties of polymers. The bio-polymers are the polymers derived from the naturally occurring renewable sources. These biopolymer electrolytes are cost-effective, and eco-friendly. These advantages have made the bio-polymer electrolytes a promising substitute for synthetic polymers in electrochemical applications. Natural biopolymers such as chitin, starch [5], pectin, carrageenan, agar-agar, methylcellulose, as well as cellulose acetate have been proposed by researchers to develop the Solid Biopolymer Electrolytes(SBE) as a cure for pollutants [6–9]. groups in its structure [10]. Among green polymers, carrageenan is one of the recommended host polymers attributed to its ability to dissolve in water without the need of using organic solvent. Carrageenan is classified into three varieties such as Iota, Lamda, and Kappa depending on the position and amounts of ester sulphate. K-carrageenan as well as I-carrageenan are considered as gel-forming carrageenan. Iota-carrageenan is made up of monomers of β-υ- galactopyranose and α-υ-galactopyranose that are joined by α-(1 → 3) and β-(1 → 4) glycosidic bridges. The nature of iota-carrageenan is flexible [9, 11–13].

Iota carrageenan comprises of hydroxyl groups where it can form cross-linking networks with other elements in the polymer electrolyte [8]. Besides, it has large distribution of oxygen atoms in the structure which help to form coordinated bond with cations [9]. Pure iota carrageenan sample shows 3.86×10^{-6} Scm^{-1} [9]. Nevertheless, after the addition of salt, iota-carrageenan polymer still has low ionic conductivity at room temperature.

Gum based polymers from a microbial, animal, plant, and marine sources are likewise polysaccharides. As water is added, the majority of gums tend to become a gel. Acacia gum [14], Gellan gum [15], Tragacanth gum [16], Guar gum [17], Moringa gum [18], and Xanthan gum [19] are some of the kinds of gums. The Acacia tree's exudate of tree gum is known as the AG or gum Arabic. Highly branched polysaccharide from acacia gum contains parts of glycoproteins. Though an emulsifier, stabilizer, and thickening ingredient, Gum Arabic is widely accessible to blend with another polymer. According to a recent study, one of the current methods frequently used to solve the low conductivity problem is plasticization of the biopolymer electrolyte system [9, 20]. In order to produce a smooth texture, more flexibility, and strengthen the chemical and mechanical durability of membranes, plasticizers are added. They can penetrate and extend the distance between molecules while reducing the polar groups of polymers [21, 22].

The prepared plasticizer incorporated SBEs are used in energy devices, such as EDLC, serving as possible substitute for traditional lithium batteries. Long lifecycle, safety, fabrication cost-effectiveness, and excellent performance are the highly desired properties of EDLC [23]. According to Manjuladevi et al. [24], primary lithium-ion battery was fabricated with 30% Pectin: 70% LiNO$_3$ electrolyte membrane and the open circuit voltage (OCV) was measured as 1.4 V. Another Biopolymer cellulose acetate with LiNO$_3$ added polymer electrolyte has reported in Monisha et al. [25].A Electrochemical cell has prepared by using the higher conductivity polymer electrolyte and the Open circuit voltage (OCV) of the manufactured lithium-ion battery is 1.8 V. Arokiamary et al. has done a research on kappa carrageenan doped LiNO$_3$.

The high biocompatibility of Iota carrageenan and Acacia gum with Ethylene glycol as plasticizer has been reported in our previous work. The optimized blend electrolyte has reported the conductivity as 2.96×10^{-4} Scm^{-1} [9]. Alkali metal salts are commonly added to achieve good conduction [26, 27] (including lithium salts). However, lithium-based ionic salts are most popular because lithium ions (Li+) are smaller in size, which leads to a high gravimetric Coulombic density. Li$^+$ ion incorporation with the polar group of the blend polymer is made possible by feeble coordination in the presence of salt LiNO$_3$ and increases the charge carriers and thereby rises the ionic conduction [25, 28].

The fabrication of symmetric capacitors and the analysis studies for this polymer blend electrolyte are novel, and researchers in this work achieve conductivity in the order of 10^{-3}.

Materials and Methods

Materials

The polymers, iota carrageenan (IC) and acacia gum were purchased from HiMedia chemicals (HiMedia Laboratories Pvt. Ltd.) and Qualigens Fine Chemicals Pvt. Ltd., respectively. The monomer of iota carrageenan (IC) has a high molecular weight of 946.8 g/mol with 99% purity, while acacia gum (AG) has a low molecular weight of 92 g/mol with SQ grade. 99% pure ethylene glycol with a molecular weight of 62.07 g/mol was purchased from Merck Specialties Private Limited. From Sisco Research Laboratories Pvt. Ltd., we got lithium nitrate (LiNO$_3$) with a molecular weight of 68.95 g/mol in AR grade (extremely pure).The solvent employed throughout the preparation was Deionized water.

Experimental Details

Plasticized biopolymer electrolytes (PBE) were prepared using the solution casting method. PBE was made using an optimum mixture of IC (60 wt%) and AG (40 wt%) with ethylene glycol (0.75 ml). Iota carrageenan was liquefied in 40 ml of deionized water for 3 h at 60 °C, and the acacia gum solution was made by using 20 ml of deionized water and stirred at room temperature for the same amount of time. To get a clear solution, these two solutions should be progressively combined and stirred for 3 h. After that, 0.75 ml of ethylene glycol was added as a plasticizer. Following that, specified concentrations of lithium nitrate ($LiNO_3$) (10%, 20%, 30%, and 40%) were dissolved utilizing 10ml of distilled water which was then agitated for 2 h at room temperature using a magnetic stirrer. The polymer blend solution was then added to this salt solution, and the mixture was stirred for 20 h. Finally, the clear solution was poured into a Petri dish and let to evaporate at 50 °C in the oven. By changing the weight proportion of salt, four different PBEs were synthesized and the preparation steps is given in Fig. 1a and the Photograph of the prepared polymer electrolyte are clearly shown in Fig. 1b. The prepared PBE has thickness ranging from 0.032 to 0.036 cm. The ratio of prepared electrolytes is shown in Table 1.

Fabrication of Electrode

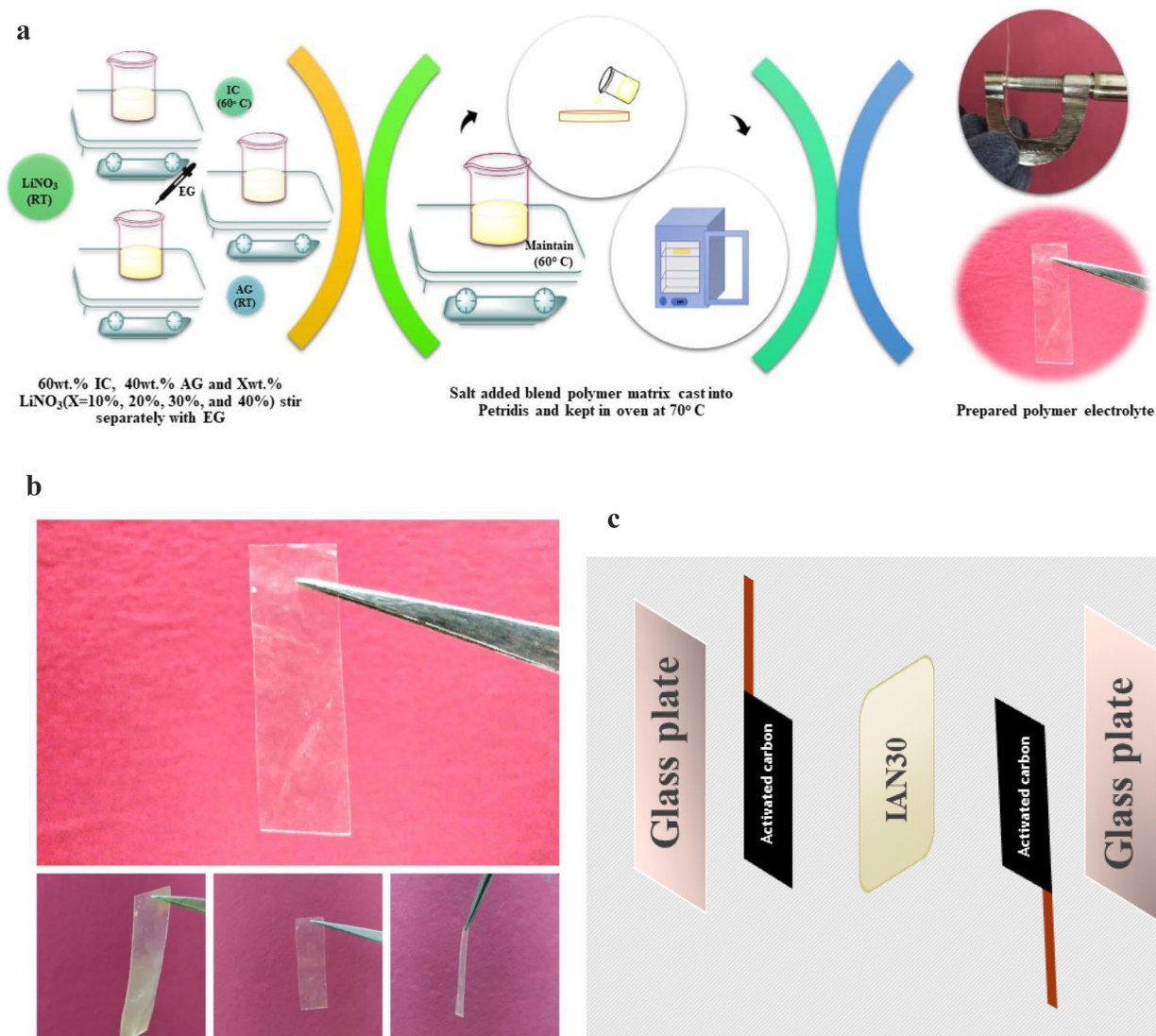The preparation of the carbon electrodes is the first stage of the EDLC preparation. The activated carbon (bought from

Fig. 1 **a** Solid biopolymer electrolyte preparation flow chart. **b** The picture of prepared electrolyte. **c** The design of fabricated symmetrical capacitor (EDLC)

Table 1 Prepared samples ratio in grams and weight%

S.no	Sample code	The ratio of IC:AG:LiNO$_3$ wt% with 0.75 ml ethylene glycol	Ratio in grams
1	IAGB	60:40:00	0.9366:0.0634:0.0000
2	IAN10	54:36:10	0.9285:0.0628:0.0086
3	IAN20	50:30:20	0.9205:0.0624:0.0170
4	IAN30	46:24:30	0.9127:0.0617:0.0255
5	IAN40	43:17:40	0.9050:0.0612:0.0331

SANWA Components, Inc.), poly (vinylidene fluoride) (PVdF) and N-methyl pyrrolidone (NMP) were taken in the ratio of 8:1:1. Then PVdF and activated carbon were mixed with NMP using mortar and pestle to obtain ahomogeneous slurry. The homogeneous slurry was pasted evenly on nickel foil and dried at 80 °C for 12 h. The prepared electrodes were stored in a desiccator filled with silica gel to remove the moister.

Characterization Techniques

X-ray Diffraction Spectroscopy

The amorphous nature of the polymer electrolyte was confirmed using a Bruker X-Ray diffractometer. This gadget was scanned with Cu-Kα radiation at a rate of 5° per minute between 2 = 10° to 60°.

Fourier Transform Infrared Spectroscopy

The SHIMADZU IR Tracer 100 spectrometer was used to detect FTIR spectra with wavenumbers ranging from 400 to 4000 cm^{-1} and a resolution of 4 cm^{-1}.

AC Impedance Spectroscopy

The ionic conductivity and dielectric tests of the polymer electrolytes were carried out using a computer-controlled HIOKI 3532-50 LCR Hitester throughout a frequency range of 42 Hz-1 MHz and a temperature range of 303–368 K.

UV/Vis Spectrophotometer

Optical properties were measured using a Beckman DU640 UV/Vis spectrophotometer in the range of 200–900 nm.

Electrochemical Performance

Electrochemical performance was investigated using cyclic voltammetry (CV) and galvanostatic charge/discharge (GCD) with the CH-Instrument Model 6008e.

Transference Number Analysis

Wagner's polarization technique was used to identify the ionic and electronic transference number.

Fabrication of Symmetric Capacitor

Symmetrical capacitors with a solid polymer electrolyte have a rapid charging/discharging rate in addition to low electrical resistance and non-combustibility [29]. In this paper, higher conducting sample IAN30 serves as an electrolyte, activated carbon (AC)-based electrode systems are used to create a symmetrical super capacitor device with the design shown below. The design of the fabricated supercapacitor is given in Fig. 1c.

EDLC: AC ‖ 60 wt% Iota carrageenan: 40 wt% Acacia gum: 30 wt% LiNO$_3$ with 0.75 ml Ethylene glycol ‖ AC.

Results and Discussion

XRD

XRD investigation is carried out to establish whether the new derivative samples are amorphous or semi crystalline. Figure 2 shows the XRD pattern of optimized blend polymer IAGB (60 wt% IC: 40 wt% AG: 0.75 ml EG) and 10 to 40 wt% LiNO$_3$ added blend polymer. The X-ray diffraction patterns of pure Iota carrageenan (IC) electrolyte exhibits hump at 2θ = 20°, 30°, and 41° and, gum acacia pure (AG) electrolyte exhibits hump at 2θ = 20° and 40°. The diffraction humps of IAGB polymer electrolyte are at 2θ = 20°, 30° and 40°.

The intensity of the diffraction hump at 2θ = 20°, 30°, and 40° decreases and wide as the concentration of LiNO$_3$ increases. It may suggested that the interaction between polymer chains and salt particles is decreased, and thereby the amorphous character is increased, which is definite by peak broadening and reduction in the intensity of hump as shown in Fig. 2. IAN30 sample attains the low intensity hump at 20°, 30°, and 40°.

There is no Crystalline peaks belongs to pure lithium nitrate (2θ = 35.4°, 46.4°, and 51.1° (JCPDS-76-0164)) for
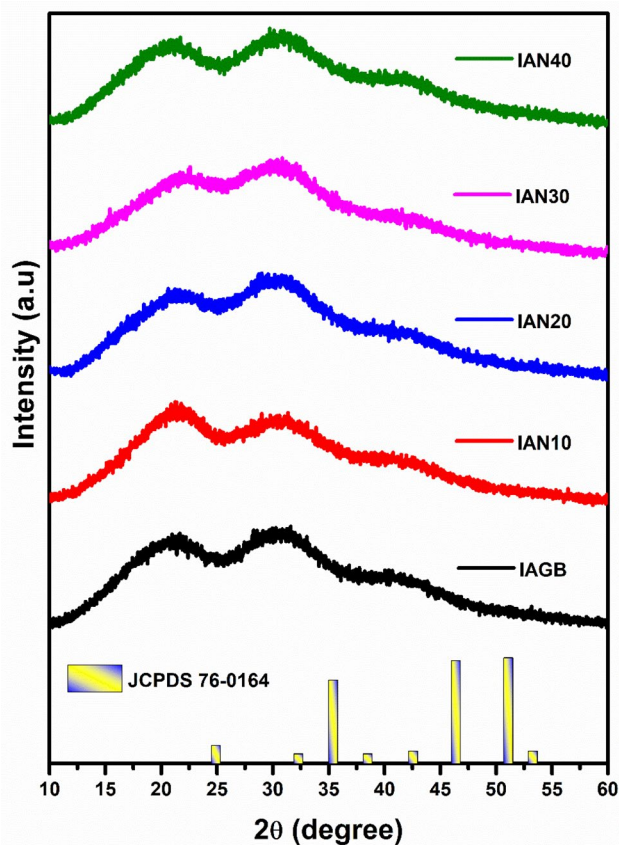
Fig. 2 X-ray diffraction pattern for all prepared samples and JCPDS pattern of LiNO₃salt

all the lithium nitrate added samples. This is a confirmation of the complete disolvation of lithium nitrate with the optimized blend.

FT-IR

Figure 3a displays the Fourier transform infrared spectra of optimized IAGB and various weight percentages of the LiNO$_3$ added system. The noted vibrational bands of the electrolytes are shown in Table 2. The O–H band assignments are observed at 3354 cm^{-1}for the IAGB sample. This O-H band is slightly shifted to 3352 cm^{-1} for salt-added samples. This shows that the oxygen atoms in the hydroxyl groups of the IC interacted with the lithium ions via ion dipole interactions [30]. In all prepared samples, the vibration band appeared at 2932 cm^{-1} is owing to alkyl group of C–H stretching due to presence of AG [31].

Figure 3b presents the vibration band of the samples range from 1800 to 600 cm^{-1} elaborately. The incorporation of LiNO$_3$ with IAGB polymer leads to the shifting of peak. While blended with 10–40 wt% of LiNO$_3$, the peak appeared at 1635 cm^{-1} is recognized as H–O–H deformation band [32].The asymmetrical and symmetrical axial vibration of the –COO group in AG [33] are indicated by the band at 1438 cm^{-1} and this band dislocates to 1453 cm^{-1}, 1458 cm^{-1}, and 1463 cm^{-1} with the increase of salt concentration. The band at 1224 cm^{-1} is relevant to S–O sulphate stretching of pure iota carrageenan(IC) [34]. For 10 wt%, 20 wt%, and 30 wt% of LiNO$_3$ added systems, this band is moved slightly.

The vibration band around 1032 cm^{-1} and 842 cm^{-1} is due to CH$_2$ asymmetric stretching and –O–SO$_3$ stretching of D-galactose-4-sulphate for all prepared electrolytes [35, 36]. In all salt-added electrolytes, there is a shift in typical peak at 1064 cm^{-1}which corresponds to C–O of 3,6-anhydrous galactose stretching and C–O stretching is observed at 977 cm^{-1}. The wavenumber of the peak at 1064 cm^{-1}
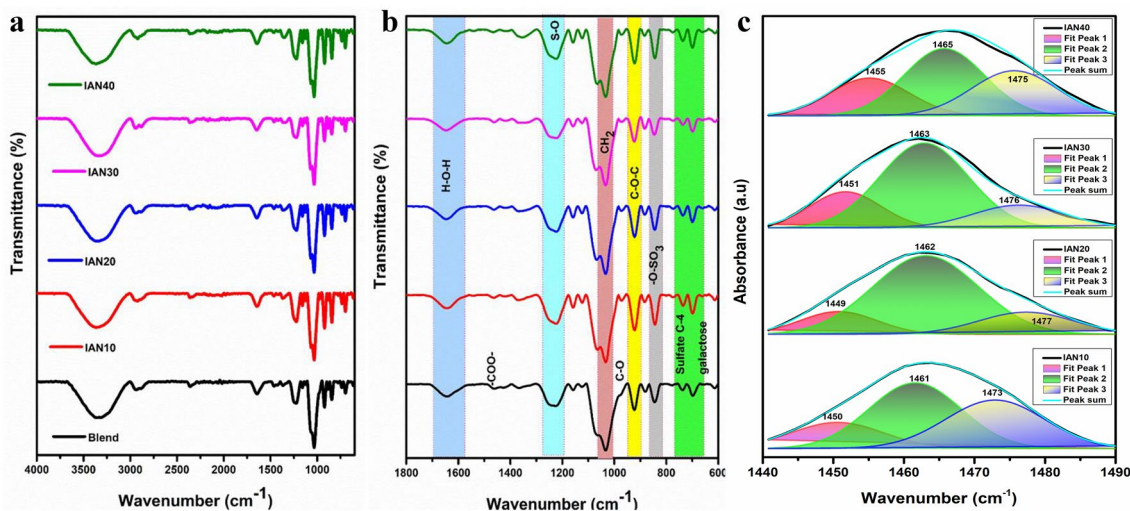

Fig. 3 a FT-IR spectra of prepared electrolytes and **b** the FT-IR spectra in the range of1800-600 cm-1 wavenumber. Deconvolution of FT-IR spectra at a wavenumber between in the range of 1440-1490cm^{-1}

Table 2 Functional group assignments for ICP, AGP, IAG, IAG01, IAG02, and IAG03

Assignment	Wave number (cm^{-1})				
	IAGB	IAN10	IAN20	IAN30	IAN40
O–H stretching	3354	3352	3352	3352	3352
C–H stretching	2932	2932	2932	2932	2932
H–O–H (Water deformation band)	1635	1639	1639	1639	1639
–COO$^-$symmetrical and asymmetrical streching	1438	1453	1458	1463	1463
S–O sulfate stretching	1224	1222	1222	1222	1220
CH$_2$ asymmetric stretching	1032	1032	1032	1032	1032
C–O stretching of 3-6 anhydro galatose stretching	1064	1070	1070	1068	1066
C–O stretching	977	970	970	970	970
C–O–C of 3-6 anhydro galatose stretching	920	922	923	925	920
–O–SO$_3$ stretching at D-galactose-4-sulphate	842	842	842	842	842
Sulfate C-4 galactose	738	732	734	734	736

is decreased as the concentration of lithium ions increased because more of the oxygen atoms (C–O) in the IC are affected by interactions with the lithium ions [37]. The peak around 920 to 925 cm^{-1} is related to the C–O–C of 3,6-anhydrous galactose stretching [32]. The vibrational band at 732 to 738 cm^{-1} corresponds to the presence of Sulfate C-4 galactose stretching in the electrolytes. In all electrolytes, the intensity of this peak increases due to increase in the amount of functional group associated with the molecular bond and also confirm the physical interaction between the iota-carrageenan, Acacia gum structure, LiNO$_3$ salt and EG [38, 39].

FTIR Deconvolution

The characteristics of ions in the prepared electrolyte are better understood using an FTIR-deconvolution method via Origin 9.1. The FTIR spectra are deconvoluted by using curve fitting and line-based correction at the chosen wavenumber region. The percentage of free and contact ions is calculated using the FTIR deconvolution technique. The –COO$^-$'s in carboxylate group causes a strong attraction towards Li$^+$ and enables the ion transportation. The region from 1440 to 1490 cm^{-1} corresponding to the carboxylate group is selected due to the nucleophilicity of the COO$^-$ which exerts an attraction towards Li$^+$ from LiNO$_3$. This allows the ion–ion interactions by the weak bonds of COO$^-$–Li–NO$_3$ in biopolymer matrices. Due to the breaking of weak bond and less ionic mass, the Li$^+$ transportation occurs mostly, which could be useful in quantifying the transport features. This pattern has suggested that a higher concentration of LiNO$_3$ dissolves into a greater number of free Li$^+$ ions, that are essentially provide conductivity [2].

The free ion peaks are appeared at 1451 cm^{-1} and 1463 cm^{-1}. Then the peak appeared at 1476 cm^{-1} is attributed to the contact ions for the electrolyte IAN30.It was possible to identify free and contact ions in that case based

on the deconvoluted area as shown in Fig. 3c [2]. The percentage of free ions and contact ions of salt observed in the COO$^-$ band region can be determined using the equation below:

$$\text{Percentage of free ion (\%)} = \left(\left(A_f / \left(A_f + A_c\right)\right)\right) \times 100, \tag{1}$$

where A_f is the total area of the free ion region and A_c is the overall area of the contact ion region based on the deconvoluted FTIR peaks. The area of deconvoluted bands is used to calculate the percentage of free ions and contact ions, and these values are tabulated in Table 4. The characteristic peaks of free ions are usually larger than the contact ions [28].

In comparison to the other concentration electrolytes, the higher conducting electrolyte (IAN30) achieves the highest percentage (82.93%) of free ions and the lowest percentage (17.07%) of contact ions (Table 3).

Cole Cole

Analyzing of electrochemical properties can be done simply and effectively using alternative current impedance spectroscopy. Figure 4a–f displays the cole cole plots for prepared polymer electrolytes with equivalent circuits. In the complex impedance plots, there exists two substantial different zones which is due to the bulky nature of the electrolytes. A

Table 3 Measured IR deconvolution free ions and contact ions percentage

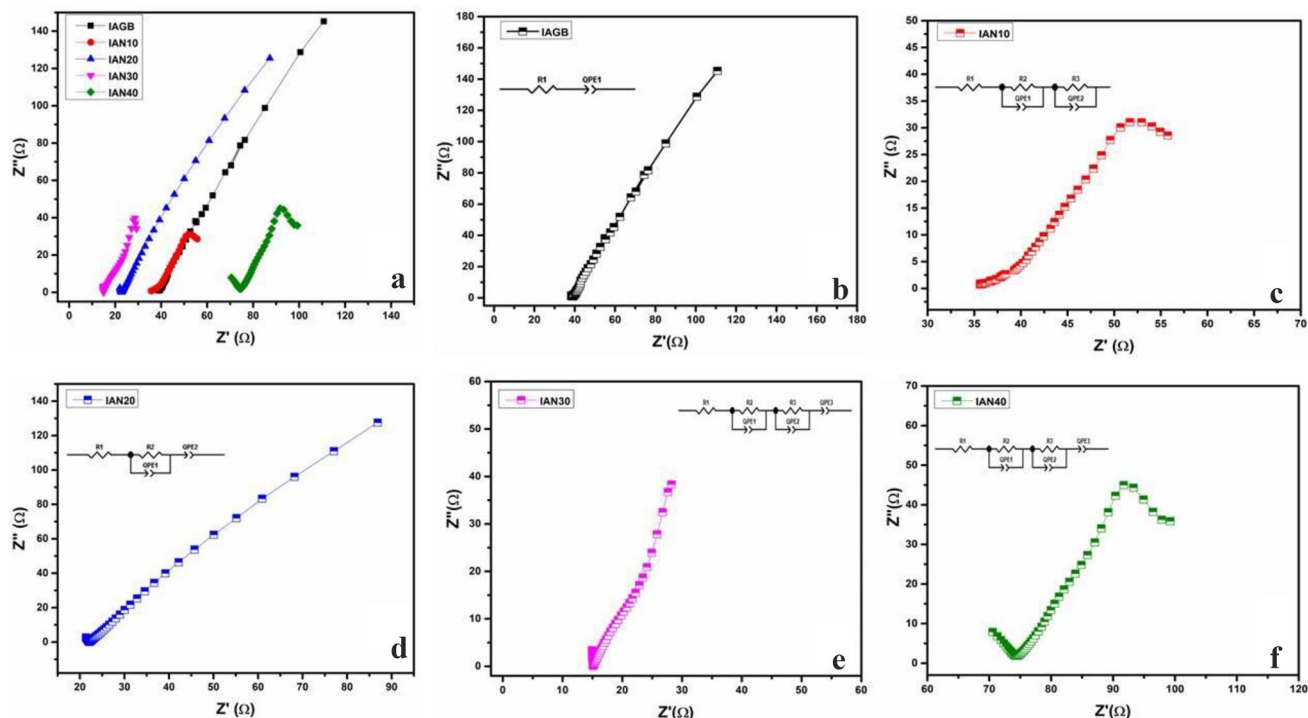| Sample code	Free ion %	Contact ion %
IAN10	62.83	37.17
IAN20	81.39	18.60
IAN30	82.93	17.07
IAN40	68.60	31.39

Fig. 4 **a–f** AC impedance spectrum with an equivalent circuit

semicircle in the high-frequency region and low-frequency spike are caused by the polarizing action in the electrolyte-electrode contact area [40–42]. Equivalent circuit modelling is the most widely used method and is accomplished by approximating the experimental data with an electrical circuit, followed by complex non-linear least squares (CNLS) fitting using ZView software. Figure 4b shows a low-frequency spike region with an equivalent circuit of series arrangement of resistance and capacitance phase elements (QPE) for the sample IAGB.

The R_b value is determined using the ZView software. The following equation has been used to determine the sample conductivity based on the value of R_b.

$$\sigma = \left(\frac{1}{R_b}\right) \times \left(\frac{t}{A}\right) S\, cm^{-1}, \tag{2}$$

where t is the electrolyte thickness, A is the electrolyte area and R_b is the bulk resistance of the electrolyte. For the IAN10 sample, two semicircle occurs with an equivalent circuit as two sets of parallel combinations of resistance (R) with QPE, as shown in Fig. 4c. For IAN20, there exists a semicircle with spike shown in Fig. 4d. The corresponding equivalent circuit is parallel combination with bulk resistance R_b with QPE for a semicircle, and also a series circuit of a different capacitor, QPE, represents a sloping spike at a lower frequency [9, 43, 44].

For IAN30 and IAN40, there exhibits two semicircles with spike fitted by an equivalent circuit of parallel combination of resistance and QPE and series combination of another QPE (Fig. 4e and f). The two semicircles occurred in IAN10, IAN30 and IAN40 is the result of increased molecular packing of Iota carrageenan polymer chain [45].Those semicircles are fitted using ZView software to obtain the resistance values. Then the resistance values are added to get the bulk resistance.

The chains are made as irregular and entwined in amorphous regions. As a result, the molecular packing in the amorphous state is weak and the molecular chains can move more easily than in the crystalline form. As a result, the chains in the amorphous phase are more malleable and may so orient themselves substantially more quickly. This allows for considerable ion mobility in the amorphous material.

However, when more than 40 wt% of LiNO$_3$ salt added into the polymer blend matrix, the intensity of the humps are increased, which leads to increase in the viscosity of the polymer electrolyte films. As a result, because there is less free space for ion transmission, charge carriers are less mobile. So that, the conductivity is reduced. Li$^+$ ions are made easier to access by the rise in amorphous form with salt weight%. This increase of amorphous nature with the increase in wt% of salt facilitates Li$^+$ ions movement in the polymer network. The absence of the peak is related to LiNO$_3$ salt concentration in the electrolyte system clearly indicating the complete

dissolution of the salt in the polymer matrix. The obtained results are in good agreement with conductivity studies in this work.

As the concentration of LiNO$_3$ salt increases, the bulk resistance (R$_b$) value decreases that is shown in Figs. 4 and 30 wt% of LiNO$_3$ added sample (IAN30) attains the minimum R$_b$ value and maximum conductivity value as 1.77×10^{-3} Scm^{-1}.

Conductance Spectra

Ion conduction and the hopping movements of the ionic charge are described by the conductance spectra for SPE. For all prepared samples, the conductance spectra is shown in.

Figure 5. It has a high-frequency plateau region and a low-frequency dispersion region. There is dispersion at lower frequencies due to the effects of the electrolyte and electrode polarization. The DC conductivity of SPE is calculated using the high-frequency plateau area. As the LiNO$_3$ salt concentration increase up to 30 wt%, the low frequency dispersive region gets prominent and shifts to a higher frequency. This is due to the improvement of free charge carriers available in the system [46].

For IAN30 electrolyte, the bulk amount of ions pass over the potential barrier as a result of the charge carriers' columbic interaction, which causes disorder in the structure and the improvement in conductivity [47, 48]. However, as salt concentration rises, association of ions begins to repeatedly to form neutral ion aggregates and reduce electrical conductivity [49], resulting in the conductivity value for the IAN40 sample decrease and also the plateau region shifts to lower frequency region.
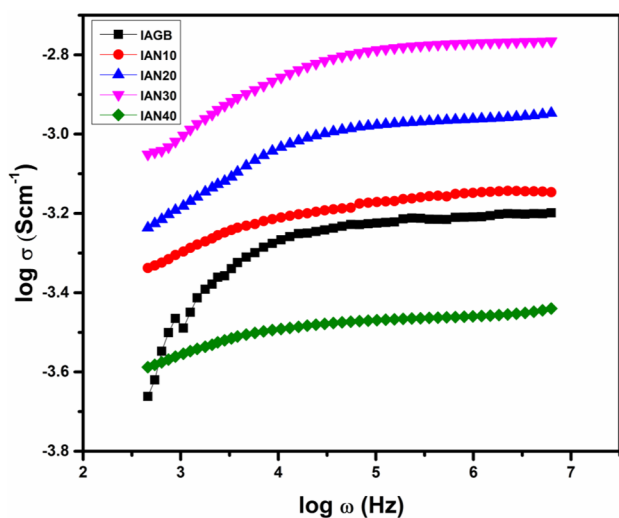
Table 4 Measured conductivity and activation energy values of all samples

Sample code	Conductivity	Activation energy (eV)
IAGB	2.96×10^{-4} S cm^{-1}	0.068
IAN10	3.49×10^{-4} S cm^{-1}	0.056
IAN20	1.00×10^{-3} S cm^{-1}	0.034
IAN30	1.77×10^{-3} S cm^{-1}	0.022
IAN40	2.11×10^{-4} S cm^{-1}	0.054

Temperature-Dependent Studies

To identify the mechanism of ionic conduction in polymer electrolytes, temperature-dependent ionic conductivity is used. The Arrhenius plots for the prepared electrolytes in the temperature range 303–338 K are shown in Fig. 6. A thermally activated process is suggested by the linear change of log σ versus 1000/T plots. The conductivity can be expressed by,

$$\sigma = \sigma_0 \exp\left(\frac{-E_a}{kT}\right), \tag{3}$$

where σ_0 is pre-exponential factor, k is the Boltzmann constant, T is the temperature in Kelvin, and E$_a$ is the activation energy [50]. By the addition of salt with the polymer blend, the ions require less energy to diffuse, migrate within the salt-added plasticized polymer electrolyte. From a result, strong plasticizing action and salt incorporation strengthen the polymeric backbone and thereby increases the conductivity [51]. The Arrhenius equation properly describes the
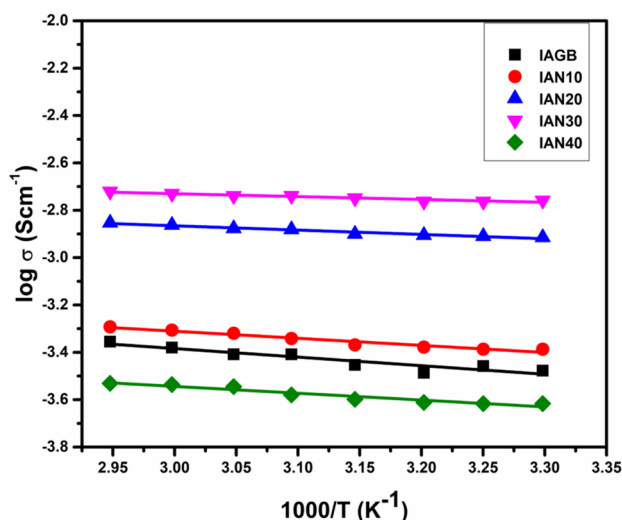

Fig. 5 Frequency dependence conduction spectra of Blend and different concentration lithium nitrate added samples

Fig. 6 Arrhenius plot of IAGB, IAN10, IAN20, IAN30, and IAN40

data in Fig. 6. The calculated activation energy and conductivity values are explained in Table 4. By the addition of 30 wt% of $LiNO_3$ to the polymer electrolytes, the activation energy significantly reduces from 0.068 to 0.022 eV. The direct relationship between ionic conductivity and activation energy value is caused by a decrease in the energy barrier for lithium ion, which directly lowers the activation energy [5, 49].

Conduction Mechanism

By using Jonscher's universal power law, it is possible to determine the electrolyte's ionic conduction mechanism. The ac conductivity patterns with rising temperature is reflected by using the Jonscher's universal power law as follows,

$$\sigma_{ac} = \sigma_{dc} + A\omega^s, \tag{4}$$

$$\omega^s = \frac{\sigma_{dc}}{A}, \tag{5}$$

where ω^s is hopping frequency and A is the temperature-dependent parameter. Typically, the power-law exponent s is less than one. According to the aforementioned calculations, higher conducting samples follow the Jonscher power law. As seen in Fig. 7, the IAN30 sample exhibits a high-frequency plateau region due to space charge polarization. Some of the theories that characterize the conduction mechanism are quantum mechanical tunnelling (QMT), correlated barrier hopping (CBH), overlapping large-polaron tunnelling (OLPT), and non-overlapping small polaron tunneling (NSPT) [9, 52, 53]. The QMT model is implied by the observation that both exponents s_1 and s_2 are temperature
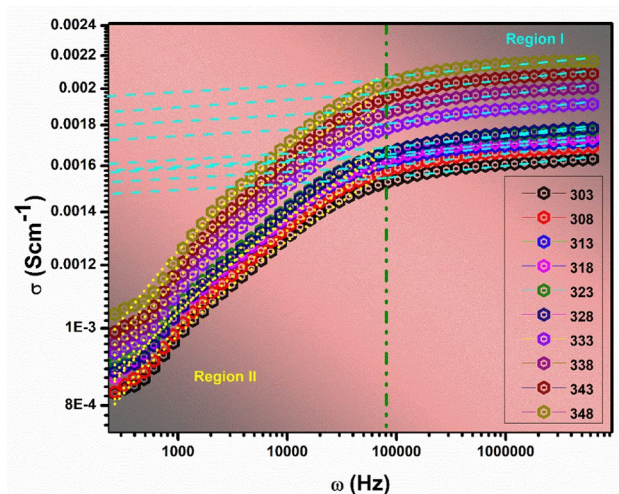
independent [54]. Figure 8a and b depicts whether the exponents s_1 and s_2 corresponding to Region I and Region II.

The corresponding fitting equation can be expressed as,

$$s_1 = 8.6E - 3T - 1.65 \times 10^{-5}, \tag{6}$$

$$s_2 = 3.9E - 3T + 2.07 \times 10^{-6}. \tag{7}$$

Studies on the QMT model have revealed that the tunneling distance appears to be temperature independent, whereas the frequency exponent parameter is not temperature dependent. Conducting ions and stress fields interact to create the polaron, which is based on quantum mechanical phenomena. That polarons tunnel through the potential barrier and travel through it. According to the QMT model, the AC conductivity is caused by either electronic or atomic tunnelling between equilibrium sites [55, 56].
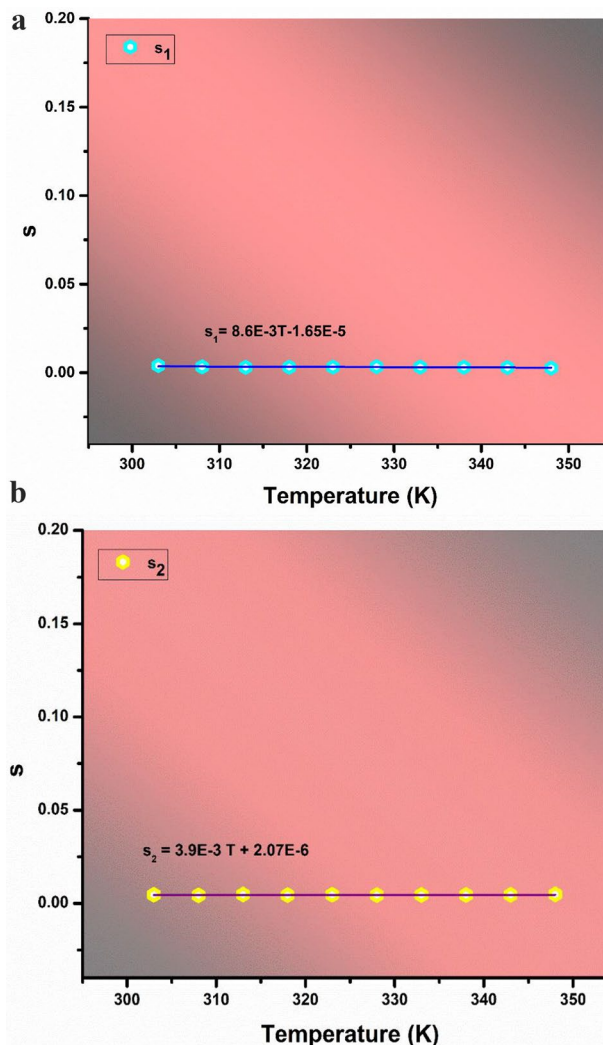

Fig. 8 Exponential s versus temperature (K)

Fig. 7 Conduction mechanism of higher conducting sample at various temperatures

Dielectric Spectra

The findings from impedance measurements are used in the current study to analyze the dielectric behavior of polymer electrolytes. The energy lost after a sudden reversal of the electric field's polarity is known as dielectric loss ε_i whereas a substance's capacity to store charge is known as the dielectric constant (ε_r). The following formulas are used to calculate the two dielectric values:

$$\varepsilon_r = \frac{Z''}{\omega C_0 \left(Z'^2 + Z''^2\right)}, \tag{8}$$

$$\varepsilon_i = \frac{Z'}{\omega C_0 \left(Z'^2 + Z''^2\right)}, \tag{9}$$

where Z′ and Z″ represents the real & imaginary impedance, ω is the angular frequency, C_0 represents the vacuum capacitance, and ε_i and ε_r are the imaginary and real permittivity. Figures 9 and 10 demonstrate how the space charge polarization causes the value of ε_i and ε_r to increase dramatically with increase of salt concentration at low frequency. By adding salt to the polymer blend matrix, the dielectric constant rises and is directly correlated with the quantity of free charge carriers. The high value of the dielectric constant and loss at the low-frequency window is due to the electrode polarization event, which is still related to the ion accumulation and shows that the salt has completely dissociated. This nature further supports the non-Debye dependence [57]. Due to the periodic reversal of the applied field, the values of ε_i and ε_r become constant at high frequencies. When a sample with 30 wt% LiNO$_3$ (IAN30) is compared to an IAGB sample, a high dielectric loss value is seen, and this may be
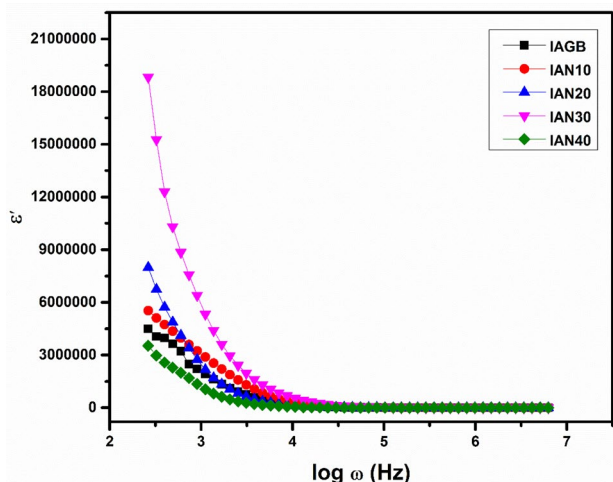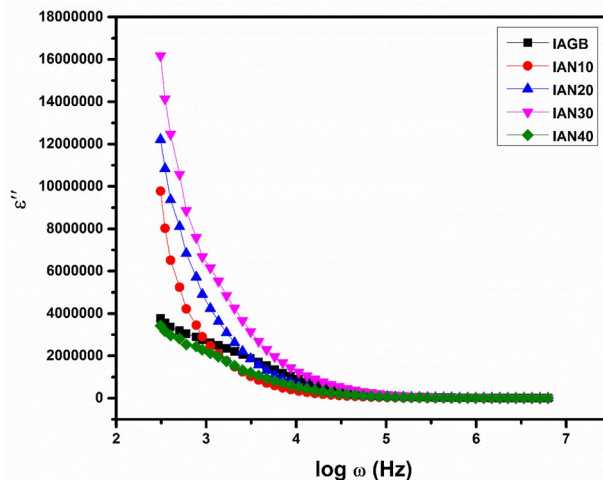

Fig. 10 Dielectric loss spectra as the function of log frequency of LiNO$_3$ doped Blend biopolymer electrolytes

explained by the electrical conductivity, which is connected to the dielectric loss. The dielectric loss is increased in the low-frequency range due to the ability of polymeric dipoles to align themselves with the applied field. Increase the salt content further, (up to 40 wt%), there exists a minimal value of dielectric loss at low frequency. However, the dipoles cannot align themselves in the direction of the applied field and diminishes the value of the dielectric loss which is almost constant in the high-frequency region [58].

Modulus Spectra

The dielectric modulus (M^*) can be determined using the formula below:

$$M^* = M' + iM'', \tag{10}$$

$$|M^*| = \sqrt{(M'^2) + \left(M''^2\right)}, \tag{11}$$

$$M' = \frac{\varepsilon_r}{\varepsilon_r^2 + \varepsilon_i^2}, \tag{12}$$

$$M'' = \frac{\varepsilon_i}{\varepsilon_r^2 + \varepsilon_i^2}, \tag{13}$$

where real and imaginary moduli are represented respectively by M′, M″. The real (M′) and imaginary (M″) parts of the modulus approaches zero at low frequencies as shown in Figs. 11 and 12, indicates the negligible impact of electrode polarization phenomena. There is a significant tail at lower frequencies as a result of the enormous capacitance connected to the electrodes. The bulk effect results in a gradual
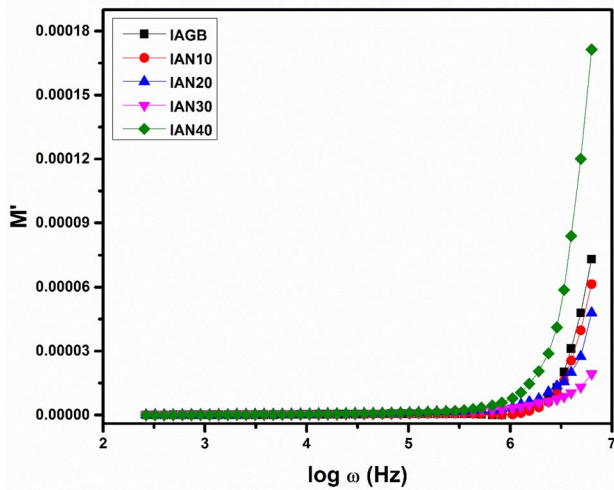

Fig. 9 Dielectric constant as the function of log frequency of LiNO$_3$ doped blend biopolymer

Fig. 11 Real modulus spectra for blend and salt added system
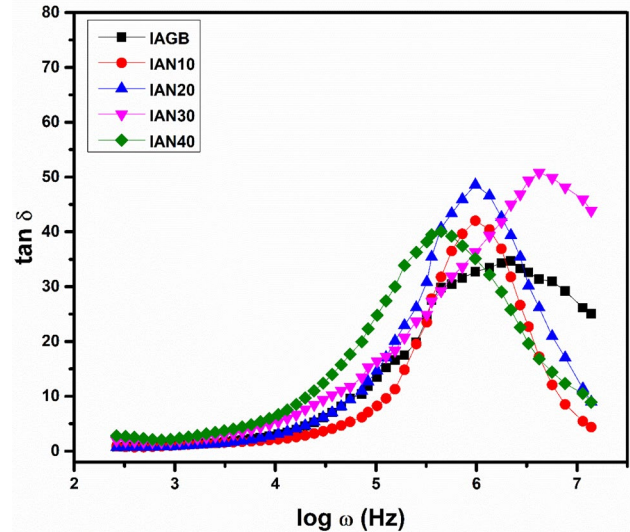
Fig. 13 Tangent spectra for all prepared samples

Table 5 Observed tangent spectra parameters

Sample	FWHM	Relaxation time (1/ω) (s)	Beta (β)
IAGB	1.42	6.71893×10^{-7}	0.8
IAN10	1.22	1.02731×10^{-6}	0.9
IAN20	1.36	1.02991×10^{-6}	0.8
IAN30	2.73	2.39883×10^{-7}	0.4
IAN40	1.68	2.09122×10^{-6}	0.6

$$\tan \delta = \frac{\varepsilon''}{\varepsilon'}. \tag{14}$$

The loss tangent vs. frequency plot for each electrolyte at room temperature is shown in.

Fig. 13. When dielectric relaxation occurs, the loss tangent peak shifts to a high-frequency area. Dipoles, whether they are induced or permanent, cause the dielectric relaxation peak. Furthermore, it is demonstrated that induced diploes also impact the relaxation function of the polarized mobile charge carriers [61]. The peaks in Fig. 13 represent the linear ion dynamics that are related to the conductivity and relaxation of the mobile ions. The relaxation time (τ) is calculated using the reciprocal of the corresponding frequency (log ω) of the greatest height of the hump and is shown in Table 5.The higher conducting electrolyte IAN30 obtains a lowest relaxation time than other electrolytes. In terms of the conductivity relaxation, the Kohlrausch–Williams–Watts (KWW) function $\phi(t)$ is given below,

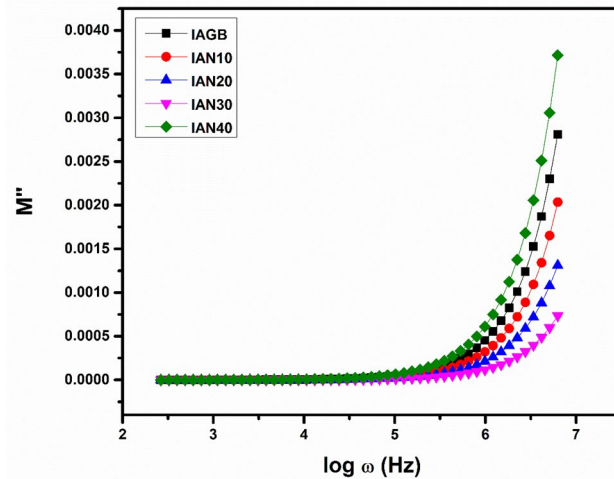$$\varphi(t) = e^{\left[-\frac{t}{\tau}\right](\beta)}. \tag{15}$$

Fig. 12 Imaginary modulus spectra for blend and salt added system

increase in modulus values with increasing frequency. This supports the non-Debye behavior of the samples [5, 59, 60].

Tangent Spectra

It is also possible to establish the frequency dependence of the dielectric loss tangent (tanδ) in order to comprehend relaxation processes. With the help of the dielectric properties, the tanδ is determined. The dissipation factor, also referred to as tan δ is frequently a ratio of energy dissipated to energy conserved in an electric field. The following equation is used to get the tanδ,

Since β is the Kohlrausch exponent parameter and is established by β = 1.14/FWHM. The non-Debye model is suggested when the calculated value of β is less than one (0 < β < 1) [55, 62]. Table 5 shows the calculated tangent spectra parameters.

UV studies—Optical Properties

Absorbance Spectra

At room temperature, UV absorbance spectra is obtained in the wavelength range of 190–900 nm by UV–Vis Spectrophotometer. As reported by Aziz et al. [63], absorbance peaks of all the electrolytes are appeared within the range of 200–250 nm wavelength. According to molecular orbital theory, absorption of light from the ground state to the higher excited state occurs with possible transitions from σ and π and n-orbitals. As a result, transitions σ → σ*, n → σ*, n → π* and π → π* take place [60]. It is possible to change the polymer electrolyte's optical properties by adding salt to the blend.

In Fig. 14, The variation of optical absorbance with wavelength is clearly illustrated. The blend electrolytes show higher absorption by the addition of $LiNO_3$ salt [64, 65]. Due to the n → π* transition, the absorbance curve is appeared in the wavelength 214–231 nm for the blend. The absorbance peaks are appeared in the range of 215–238 nm for the salt added plasticized polymer electrolytes. The appeared peaks are shifted to higher wavelength with the increase in salt concentration. The absorption coefficient must be analyzed to know about the possibility of any band structure modifications [66, 67]. The absorption coefficient ′α′ is calculated using the following equation,

Fig. 14 Optical absorption spectra for blend and different weight percentage of $LiNO_3$ added samples

$$\alpha = \frac{2.303}{d} \times A, \tag{16}$$

where 'A' is the absorption and 'd' is the sample thickness [5, 6].

Optical Band Gap Energy

The optical band gap energy (E_g) is typically observed through an optical investigation. When a photon is absorbed by a polymer electrolyte, a transition takes place in the band gap region. The Tauc's plot is plotted in Fig. 15a–e for the different 'n' values and the band gap energy (E_g) values are calculated. There exists a variation in the band gap energy with the addition of $LiNO_3$ is observed. The optical band gap energy (allowed, forbidden, direct, and indirect) is one of the optical parameter that may be calculated using these absorbance characteristics [68]. The formula used to calculate the optical band gap energy is given by,

$$\alpha h\nu = A \left(h\nu - E_g \right)^n, \tag{17}$$

where "E_g" stands for photon energy, "α" for absorbance coefficient, "A" for constant, and "n" for the type of transition [69]. The n values for direct allowed, indirect allowed, direct forbidden, and indirect forbidden transitions are denoted as 1/2, 2, 3/2, and 3 respectively. Plotting the graphs between photon energy and $(\alpha h\nu)^n$ gives the optical band gap energy. The optical dielectric loss parameter and the Tauc's model should be compared in order to determine the band gap and comprehend electron transition events [70].

Figure 15e gives the band gap values by plotting the graph between Photon energy (E_g) and optical dielectric loss [71]. Table 6 presents the values in tabular form. Direct transitions happen when the electrons' wave vector is constant. An indirect transition occurs if the lowest site of the conduction band is located at separate part of the k-space from the valence band, at which point the interaction with a lattice vibration actually occurs [70]. Comparing all the band gap energy values with the dielectric band gap energy value, the indirect forbidden transition (n = 3) values are calculated as 5.355, 5.069, 5.00, and 5.148 eV which is similar to the dielectric band gap energy values 5.387, 5.096, 5.029 and 5.11 eV for the samples IAN10, IAN20, IAN30, and IAN40 respectively. Thus, we conclude that the indirect forbidden transition is taken place in the prepared samples.
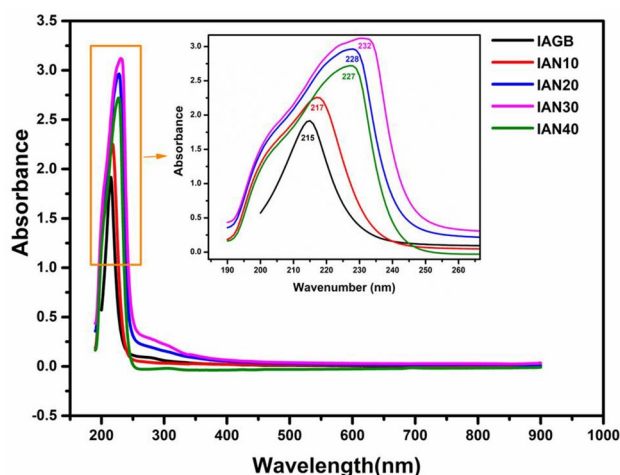
Transference Number Analysis

Transference numbers are evaluated using Wagner's DC polarization technique using blocking electrodes. In this technique, the setup is made by the configuration as one
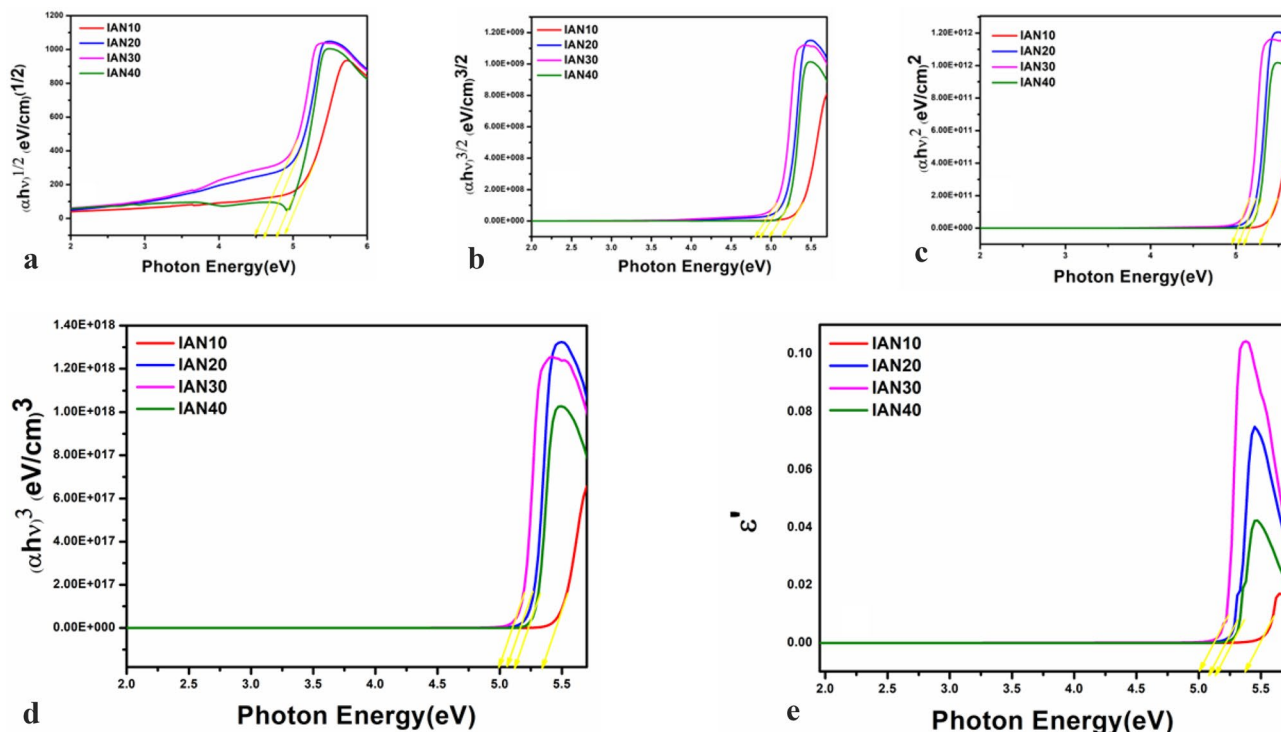
Fig. 15 Optical band gap energy of various n values **a** n=1/2 **b** n=3/2 **c** n=2 **d** n=3 and 15 **e** dielectric band gap energy for different weight percentages of LiNO$_3$added samples

Table 6 Comparison of different n values band gap energy with dielectric band gap energy

S.No	Sample	Direct-allowed band gap (n=1/2)	Direct-forbidden band gap (n=3/2)	Indirect-allowed band gap (n=2)	Indirect-forbidden band gap (n=3)	Dielectric band gap (eV)
1	IAN10	4.905	5.155	5.293	5.355	5.387
2	IAN20	4.629	4.892	5.042	5.069	5.096
3	IAN30	4.515	4.816	4.969	5.000	5.029
4	IAN40	4.781	5.007	5.113	5.148	5.111

side graphite-coated silver electrode ‖ solid polymer electrolyte ‖ silver electrode. A dc potential of 2 V is applied over this setup. Current is taken as a function of time until constant state is appeared. The initial current is decreased with increase of time [33] [25] which is shown in Fig. 16. The t$_{ion}$ and t$_{ele}$ values are calculated by using the formula.

$$t_{ion} = I_i - I_f/I_i, \tag{18}$$

$$\mathbf{t_{ele} = I_f/I_i}, \tag{19}$$

where **t$_{ion}$** represents transport number of ions, **t$_{ele}$** represents transport number of electron, **I$_f$** represents final current, **I$_i$** represents initial current [72].

The graphite-coated silver electrode is used to block the ions, the high initial current is the result of transmission through both ions and electrons, but the final saturation current is completely caused by electron conduction [73]. The calculated transference numbers of the prepared electrolytes are listed in Table 7. The ionic transport number is 0.999 for higher conducting sample IAI30. This value is closer to unity. From this, it is confirmed that ionic transport is higher than electronic transport for prepared electrolyte.

Transference number (t$_{ele}$ and t$_{ion}$) and Conductivity (σ) are used to calculate the following parameters

$$D = D_+ + D_- = KT\sigma/ne^2, \tag{20}$$

$$n = (N_\rho \times molar\ ratio\ of\ salt)/molar\ weight\ of\ the\ salt, \tag{21}$$
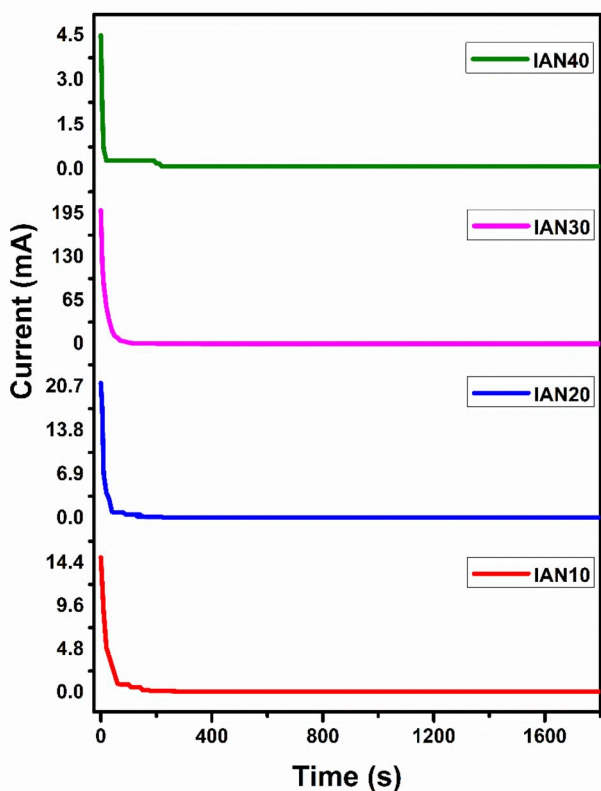
Fig. 16 Wagner DC polarization curve of IAN10, IAN20, IAN30 and IAN40 at ambient temperature

$$t_{ion} = (D_+)/(D_+ + D_-), \qquad (22)$$

$$t_{ele} = (D_-)/(D_+ + D_-), \qquad (23)$$

$$\mu = \mu_+ + \mu_- = \sigma/ne, \qquad (24)$$

$$t_{ion} = \mu_+/\mu_+ + \mu_-, \qquad (25)$$

$$t_{ele} = \mu_-/\mu_+ + \mu_-, \qquad (26)$$

where D = Diffusion coefficient (cm^2/s) K = Boltzmann constant (1.3806×10^{-23} m^2 kg s^{-2} K^{-1}), σ = Conductivity of the sample (S cm^{-1}), e = Charge of the electron (1.602×10^{-19} C), μ = Mobility (cm^2/Vs), n—Number of charge carriers, N = Avogadro's number (6.023×10^{23} particles per mole), ρ = Density of the salt (LiNO$_3$ = 2.38 g/cm^3).

The conductivity increases up to 30 wt% of LiNO$_3$ added system and a similar pattern is seen in the diffusion co-efficient and ionic mobility of cations and anions which is displayed in.

Table 7. Accordingly, values of D$_+$ and μ$_+$ for cations are higher than the values of D$_-$ and μ$_-$ for anions. The diffusion co-efficient and ionic mobility induce the higher ionic conductivity [74]. This suggests that ions are primarily responsible for the charge transport in all these polymer electrolyte films. Ion–ion and polymer-ion interactions may have an impact on the macroscopic transport parameters, which would explain by the high transference number [75]. As reported in Asnawi ASFM et al., the polymer electrolyte system of chitosan/dextran-NaTf with12 wt% of glycerol has attained maximum DC ionic conductivity and t_{ion} value as 6.10×10^{-5} Scm^{-1} and 0.988 respectively [62]. Dextran/ and chitosan/42 wt % LiClO$_4$: glycerol–based solid polymer electrolytes attained the conductivity as 4.16×10^{-4} Scm^{-1} and t_{ion} value as 0.948 [76]. Compared the previous reports, Iota carrageenan/Acacia gum/LiNO$_3$/Ethylene glycol blend polymer electrolyte has attained the improved conductivity and t_{ion} value as 1.77×10^{-3} Scm^{-1} and 0.999 respectively(See Fig. 17).

Electrochemical Analysis of Symmetrical Capacitor

Cyclic Voltammetry

A symmetrical capacitor has fabricated by using the higher conducting solid polymer electrolyte and their electrochemical performance has analyzed by cyclic voltammetry (CV) method. Figure 17a depicts the CV curve of a

Table 7 Mobility and diffusion coefficient of prepared solid polymer electrolyte

| Weight of salt in %	No. of charge carriers (n) in cm^{-3}	Transference number		Diffusion co-efficient in cm^2/s			Mobility (μ) in cm^2/Vs		
		T$_{ion}$	T$_{ele}$	D	D$_+$	D$_-$	μ	μ$_+$	μ$_-$
10	1.03×10^{20}	0.993	0.007	5.53×10^{-7}	5.49×10^{-7}	3.70×10^{-9}	2.11×10^{-5}	2.10×10^{-5}	1.42×10^{-7}
20	2.06×10^{20}	0.995	0.005	7.92×10^{-7}	7.88×10^{-7}	3.72×10^{-9}	3.03×10^{-5}	3.01×10^{-5}	1.44×10^{-7}
30	3.09×10^{20}	0.999	0.001	9.32×10^{-7}	9.34×10^{-7}	4.67×10^{-10}	3.57×10^{-5}	3.57×10^{-5}	1.79×10^{-8}
40	4.13×10^{20}	0.977	0.022	8.35×10^{-7}	8.17×10^{-7}	1.86×10^{-9}	3.19×10^{-5}	3.12×10^{-6}	7.12×10^{-8}
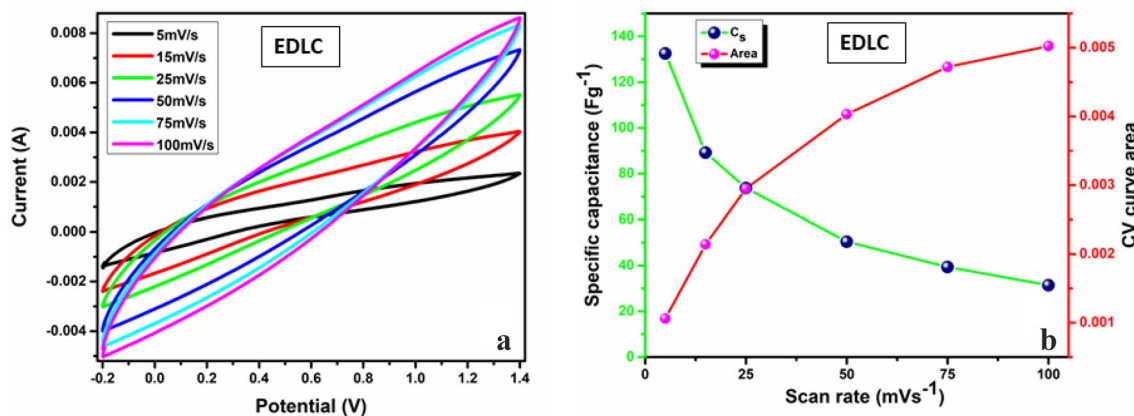
Fig. 17 **a** CV curves of devices at different scan rates; **b** Comparison of specific capacitance and area for the devices

symmetric capacitor at various scan rates of 5-100 mV/s in a potential window covering − 0.2 to 1.4 V.

The CV plot displays the leaf shape which is indicative of typical electric double layer capacitor (EDLC) behavior and the specific capacitance of the designed EDLC has been determined using the following equation:

$$C_{spe} = \frac{\int_{V_i}^{V_f} IdV}{vm(V_f - V_i)}, \tag{27}$$

where the initial and final voltages, respectively, are denoted by V_i and V_f. The active material's mass, scan rates, and the actual area of the CV curve are all denoted by the letters m, v, and $\int_{V_i}^{V_f} IdV$, respectively [77].

The lack of a redox peak in the CV profile is caused due to the diffusion of the anions and cations from the $LiNO_3$ salt at the interface of the activated carbonic electrodes rather than intercalation/deintercalation process. As a result of non-Faradaic reaction, ions are accumulated as charge double layer using electrons from activated carbonic electrodes based on potential energy. The leaf like form of CV curve is satisfactory instead of being perfect rectangular, when internal resistance and electrode roughness are considered [73].

The calculated specific capacitance (C_s), at different scan rate are tabulated in.

Table 8. The loop's surface area increases along with the scan rate due to the effective migration of ions. Due to the decreased resistance, the CV graph's surface area increases. Hence the higher conducting sample IAN30 is suitable to store energy as EDLC.

Figure 17b clearly explained about the relation between specific capacitance and curve area with scan rate. The value of specific capacitance (C_s) of the device is

Table 8 The calculated device's, specific capacitance, power density, energy density, and area

Cyclic voltametric	Galvanostatic charge–discharge (GCD)		
C_s (F/g)	C_s (F/g)	Power density (W/kg)	Energy density (Wh/kg)
31.41	22.86	1000	4.44
39.34	15.87	1100	3.09
50.39	12.02	1200	2.33
73.75	9.29	1300	1.806
89.22	5.01	1400	0.972
132.46	4.51	1500	0.875

decreased while the scan rates are increased. At a low scan rate of 5 mV/s, the specific capacitance value of EDLC is 132.46 Fg^{-1}.

Galvanostatic Charge Discharge Curve (GCD)

Figure 18a and b displays the GCD curves and current density vs. specific capacitance of the prepared symmetrical capacitor. Due to the low electrolyte resistivity of a system, a discharge begins at a certain potential window relative to its current density. A slight potential drop (self-discharge) is observed at the beginning of the discharge curve.

The most important elements in the performance of electrochemical supercapacitors are the specific energy density and power density. Power density is the amount of power in a given mass, and energy density (E_d) is the quantity of energy in a given mass (or volume). A system can store a lot of energy in a relatively small amount of mass if it has a high energy density. Power density is not always correlated with energy density. Even though it has a low power density,
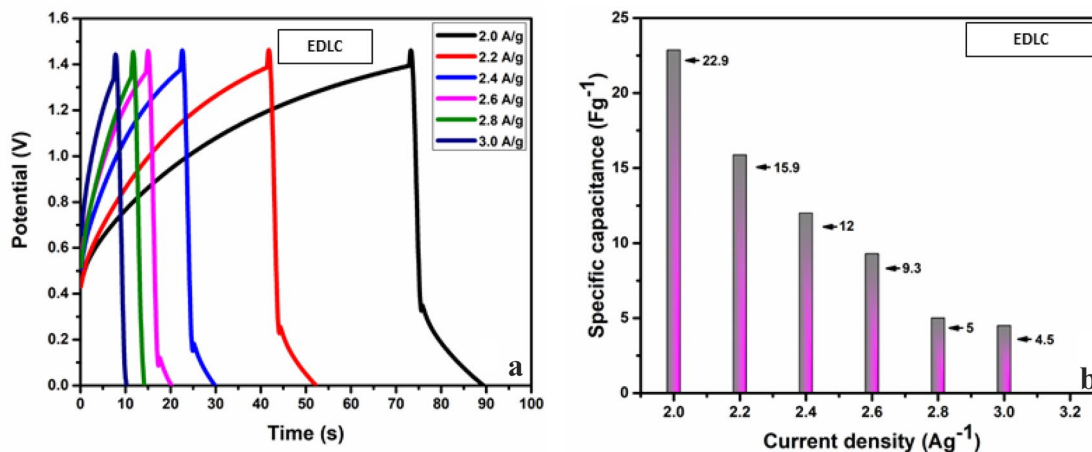
Fig. 18 a GCD curves of devices at different current density. **b** Current density vs specific capacitance relation of EDLC

a device with a high energy density can work for a considerable amount of time.

The energy and power density are calculated from the following relation,

$$E = \frac{1}{2}CV^2, \tag{28}$$

$$P = \frac{E}{\Delta t}, \tag{29}$$

where E—energy density (Wh kg^{-1}) and P—power density (W kg^{-1}). Δt—discharging time (s), V—potential window (V). The measured energy density and power density are shown in Table 8.

The equivalence series resistance (ESR) or internal resistance of the fabricated symmetric capacitor is calculated by using the following relation.

$$ESR = V_d / i, \tag{30}$$

where V_d stands for the voltage drop. The ESR value is plotted versus cycle counts up to 100 cycles in Fig. 19. This ought to be stated that the ESR value during the first cycle is 420 ohm. It gradually increases as the cycle number increases until the cycle number reaches its 50th cycle. The increase in the V_d value is the main reason for the ESR value to increase. The charge-discharge method, the gap between the electrodes and the utilized polymer electrolyte for the current collector are the major causes of the internal resistance in the fabricated symmetrical capacitor [4].

The E_d value at the first cycle was determined to be 0.87 Wh kg^{-1} according to Fig. 20. Beyond this point, the E_d values are decrease and then essentially constant with a mean value of 0.45 Wh kg^{-1} at 50th cycle. According to this, the energy barrier for anions and cations to transfer
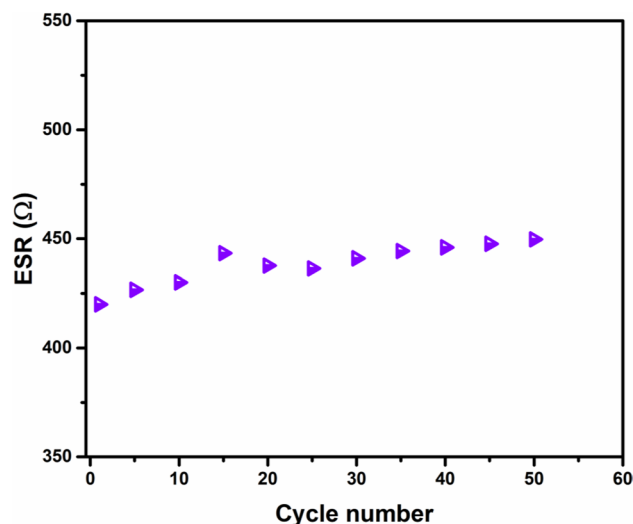

Fig. 19 The ESR value against cycle numbers up to 50 cycles

in the electrolyte is essentially the same from the first to the fiftieth cycle. Due to an increase in the ESR value, the E_d value slightly decreased during the course of 50 cycles. Therefore, the amount of stored energy lost throughout the charge–discharge cycles increases.

At the first cycle, the power density (P_d) is 1500 W kg^{-1}. After that, a charge-discharge process causes the P_d value to steadily constant shown in Fig. 21. These could be connected to the electrolyte's depletion. Rapid charge–discharge caused ion aggregations to develop, that prevented ions from being transported to the electrode surface. The ions adsorption consequently decreases at the electrode and electrolyte contacts [3, 78, 79].

As discussed in Aziz et al., the fabricated EDLC device using chitosan (CS): poly (ethylene oxide) (PEO): LiClO$_4$ electrolyte system shows a specific capacitance of 6.88 Fg^{-1},
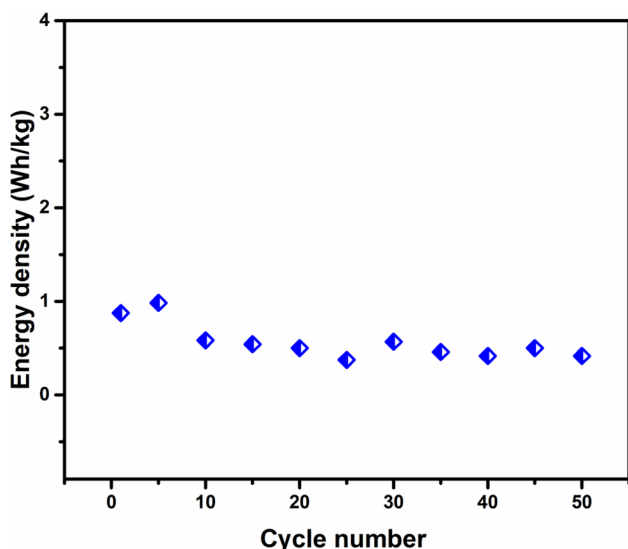
Fig. 20 Energy density (Ed) for the fabricated symmetric capacitor throughout 50 cycles
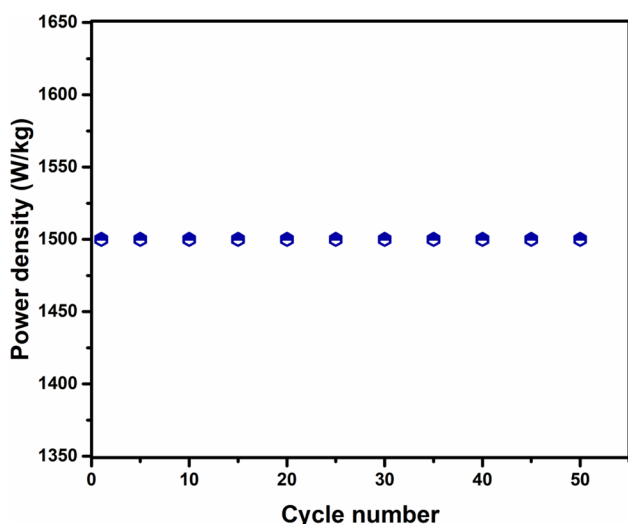

Fig. 21 Power density (Pd) for the fabricated symmetric capacitor throughout 50 cycles

power density and energy density as 305 W kg^{-1} and 0.94 Wh kg^{-1} for complete 100 cycles respectively at a current density of 0.5 mA cm^{-2} [6]. As compared to the above one, the fabricated symmetric capacitor performs well and the obtained specific capacitance is 22.89 Fg^{-1} at 0.20 Ag^{-1} current density. The attained galvanostatic charge–discharge time (Δt) is 16 s. The values for energy density and power density are 1000 Wh kg^{-1} and 4 W kg^{-1}, respectively. The results reveal the fact that the minimal current density gives a higher energy density and vice versa. Hence the higher conducting polymer electrolyte is suitable for EDLC application.

Conclusions

Biopolymer electrolyte based on optimized 60wt% Iota carrageenan:40 wt% Acacia gum: 0.75 ml Ethylene glycol blend incorporated with various wt% of LiNO$_3$ have been created using the solution casting method. The presence of LiNO$_3$ in the polymer blend brings down the peak's intensity, which in turn increases the amorphous character of polymer electrolytes. According to the XRD spectra of all of the synthesized samples. Functional groups reveal the insertion of alkali metal (LiNO$_3$) that arises from wave number shifts in the FTIR analysis. From FTIR deconvolution, the higher conducting sample attains higher percentage of free ions (82.93%) and lower percentage (17.07%) of contact ions. All prepared samples' impedance plots were fitted with equivalent circuits using the ZView program. An impedance investigation reveals that the presence of LiNO$_3$ causes a reduction in resistance value. The IAN30 sample's conductivity is increased to 1.77×10^{-3} S cm^{-1}, and the relaxation time decreases to 2.39×10^{-7} s. All prepared biopolymer electrolytes follow Arrhenius's behavior, as shown by the temperature-dependent conductivity graph. The QMT conduction mechanism is followed by the high-conducting electrolyte. Dielectric results showed that all samples' dielectric permittivity constant & loss both increase as LiNO$_3$ wt% increases. Modulus investigations revealed the impact of electrode polarization. Wagner's polarization method confirmed the high ionic transport from high cationic number of 0.999 for IAN30 sample. After examining the optical properties of the electrolytes, it is discovered that the lower band gap value of IAN30 is 5 eV. This complements the higher conducting sample's minimum band gap than other samples. The higher conducting electrolyte has used for the fabrication of Symmetrical electric capacitor (EDLC) and Electrochemical cell. The CV curves for the Symmetrical capacitor reveal the non-faradaic reaction and are found to be suitable for energy storage applications. A maximum power density of 1000 W/ kg and energy density of 4 Wh/kg are reached for EDLC at 2 A/g current density. Ultimately, it is concluded that the higher conducting electrolyte is a worthy candidate for symmetrical capacitor applications. As a part of the future work, it is advisable to select the metal organic framework as electrode materials because of its very high porosity and thereby high surface area and super performance is attained. To improve the performance of electrolytes, it is preferable to incorporate theionic liquid with the biopolymer. The ionic liquids can contribute to the increase of the concentration of cations and thus to the overall conductivity of the polymer salt complexes.

Data Availability The datasets used and/or analyzed during the current study are available from the corresponding author on reasonable request.

Declarations

Conflict of interest On behalf of all authors, the corresponding author states that there is no conflict of interest.

Ethical Approval Not applicable.

References

1. Vanitha D, Bahadur SA, Nallamuthu N, Athimoolam S, Manikandan A (2017) Electrical impedance studies on Sodium Ion conducting Composite Blend Polymer Electrolyte. J Inorg Organomet Polym Mater 27:257–265. https://doi.org/10.1007/s10904-016-0468-6
2. Zulkifli A, Saadiah MA, Mazuki NF, Samsudin AS (2020) Characterization of an amorphous materials hybrid polymer electrolyte based on a LiNO3-doped, CMC-PVA blend for application in an electrical double layer capacitor. Mater Chem Phys 253:123312. https://doi.org/10.1016/j.matchemphys.2020.123312
3. Hadi JM, Aziz SB, Kadir MFZ, El-badry YA, Ahamad T, Hussein EE, Asnawi ASFM, Abdullah RM, Alshehri SM (2021) Design of plasticized proton conducting Chitosan: Dextran based biopolymer blend electrolytes for EDLC application : Structural, impedance and electrochemical studies. Arab J Chem 14:103394. https://doi.org/10.1016/j.arabjc.2021.103394
4. Hadi JM, Aziz SB, Saeed SR, Brza MA (2020) Investigation of ion transport parameters and electrochemical performance of plasticized biocompatible chitosan-. based proton conducting polymer composite electrolytes
5. Nandhinilakshmi M, Vanitha D, Nallamuthu N, Anandha Jothi M, Sundaramahalingam K (2022) Structural, electrical behavior of sodium ion-conducting corn starch–PVP-based solid polymer electrolytes. Polym Bull. https://doi.org/10.1007/s00289-022-04230-1
6. Aziz SB, Hamsan MH, Brza MA, Kadir MFZ, Abdulwahid RT, Ghareeb HO, Woo HJ (2019) Fabrication of energy storage EDLC device based on CS:PEO polymer blend electrolytes with high Li + ion transference number. Results Phys 15:102584. https://doi.org/10.1016/j.rinp.2019.102584
7. Pawlicka A, Donoso JP (2010) Polymer electrolytes based on natural polymers. Polym Electrolytes Fundam Appl. https://doi.org/10.1533/9781845699772.1.95
8. Selvalakshmi S, Mathavan T, Selvasekarapandian S, Premalatha M (2018) Effect of ethylene carbonate plasticizer on agar–agar: NH4Br-based solid polymer electrolytes. Ionics (Kiel) 24:2209–2217. https://doi.org/10.1007/s11581-017-2417-y
9. Nandhinilakshmi M, Vanitha D (2022) Investigation on conductivity and optical properties for blend electrolytes based on iota-carrageenan and acacia gum with ethylene glycol. J Mater Sci Mater Electron. https://doi.org/10.1007/s10854-022-08925-z
10. Torres FG, De-la-Torre GE (2021) Algal-based polysaccharides as polymer electrolytes in modern electrochemical energy conversion and storage systems: a review. Carbohydr Polym Technol Appl 2:100023. https://doi.org/10.1016/j.carpta.2020.100023
11. Moniha V, Alagar M, Selvasekarapandian S, Sundaresan B, Hemalatha R (2019) Development and characterization of biopolymer electrolyte iota-carrageenan with ammonium salt for electrochemical application. Mater Today Proc 8:449–455. https://doi.org/10.1016/j.matpr.2019.02.135
12. Nithya M, Alagar M, Sundaresan B (2020) Science & technology development of red seaweed extracted film for energy saving batteries. J Integr Sci Technol 8:1–5
13. Necas J, Bartosikova L (2013) Carrageenan: a review. Vet Med (Praha). https://doi.org/10.17221/6758-VETMED
14. Elzain EMI, Mariod AA (2018) 8-Analytical techniques for new trends in gum Arabic (GA) research. Elsevier, Amsterdam. https://doi.org/10.1016/B978-0-12-812002-6/00008-7
15. Noor ISM, Majid SR, Arof AK, Djurado D, Claro Neto S, Pawlicka A (2012) Characteristics of gellan gum-LiCF3SO3polymer electrolytes. Solid State Ionics 225:649–653. https://doi.org/10.1016/j.ssi.2012.03.019
16. Jenova JSD, Venkatesh I, Karthikeyan K, Madeswaran S, Aristatil S, Prabu G, Moni (2021) Solid polymer electrolyte based on tragacanth gum-ammonium thiocyanate. J Solid State Electrochem 25:2371–2383. https://doi.org/10.1007/s10008-021-05016-7
17. Abirami M, Saratha R, Shilpa R, Vinitha B (2020) Preparation and characterization of Guar gum-based solid biopolymer electrolyte doped with lithium bis(trifluoromethanesulphonyl)imide (LiTFSI) plasticized with glycerol. Bull Mater Sci 43:6–11. https://doi.org/10.1007/s12034-020-02218-z
18. Grewal P, Mundlia J, Ahuja M (2019) Thiol modi fi ed Moringa gum—a potential bioadhesive polymer. Carbohydr Polym 209:400–408. https://doi.org/10.1016/j.carbpol.2018.12.100
19. Pawlicka A, Tavares FC, Dörr DS, Cholant CM, Ely F, Santos MJL, Avellaneda CO (2019) Dielectric behavior and FTIR studies of xanthan gum-based solid polymer electrolytes. Electrochim Acta 305:232–239. https://doi.org/10.1016/j.electacta.2019.03.055
20. Narinder Arora VS, Rajesh Kumar RK (2018) Conductivity modi fi cation of gum acacia-based gel electrolytes. Emerg Mater Res 7:89–94
21. Chai MN, Isa MIN (2013) Electrical characterization and Ionic Transport Properties of Carboxyl Methylcellulose-Oleic Acid Solid Polymer Electrolytes. Int J Polym Anal Charact 18:280–286. https://doi.org/10.1080/1023666X.2013.767033
22. Chai MN, Isa MIN (2016) Novel Proton Conducting Solid Biopolymer Electrolytes based on Carboxymethyl Cellulose Doped with oleic acid and plasticized with glycerol. Nat Publ Gr 6:1–7. https://doi.org/10.1038/srep27328
23. Aziz SB, Brza MA, Hamsan MH, Kadir MFZ, Muzakir SK, Abdulwahid RT (2020) Effect of ohmic-drop on electrochemical performance of EDLC fabricated from PVA:dextran:NH4I based polymer blend electrolytes. J Mater Res Technol 9:3734–3745. https://doi.org/10.1016/j.jmrt.2020.01.110
24. Manjuladevi R, Shilpa R, Saratha R, Selvasekarapandian S, Mangalam R (2019) Conductive bio-polymer electrolyte with lithium salt for application in electrochemical device. AIP Conf Proc. https://doi.org/10.1063/1.5130230
25. Monisha S, Mathavan T, Selvasekarapandian S, Benial AMF, latha MP, (2017) Preparation and characterization of cellulose acetate and lithium nitrate for advanced electrochemical devices. Ionics (Kiel) 23:2697–2706. https://doi.org/10.1007/s11581-016-1886-8
26. Prabakaran P, Manimuthu RP (2016) Enhancement of the electrochemical properties with the effect of alkali metal systems on PEO/PVdF-HFP complex polymer electrolytes. Ionics (Kiel) 22:827–839. https://doi.org/10.1007/s11581-015-1618-5

27. Floriańczyk Z, Such K, Wieczorek W, Wasiucionek M (1991) Highly conductive poly(ethylene oxide)-poly(methyl methacrylate) blends complexed with alkali metal salts. Polym (Guildf) 32:3422–3425. https://doi.org/10.1016/0032-3861(91)90548-W

28. Fuzlin AF, Bakri NA, Sahraoui B, Samsudin AS (2020) Study on the effect of lithium nitrate in ionic conduction properties based alginate biopolymer electrolytes. Mater Res Express. https://doi.org/10.1088/2053-1591/ab57bb

29. Ngai KS, Ramesh S, Ramesh K, Juan JC (2016) A review of polymer electrolytes: fundamental, approaches and applications. Ionics (Kiel) 22:1259–1279. https://doi.org/10.1007/s11581-016-1756-4

30. Mobarak NN, Jumaah FN, Ghani MA, Abdullah MP, Ahmad A (2015) Carboxymethyl Carrageenan based Biopolymer Electrolytes. Electrochim Acta 175:224–231. https://doi.org/10.1016/j.electacta.2015.02.200

31. Karthikeyan S, Selvasekarapandian S, Premalatha M, Monisha S, Boopathi G, Aristatil G, Arun A, Madeswaran S (2017) Proton-conducting I-Carrageenan-based biopolymer electrolyte for fuel cell application. Ionics (Kiel) 23:2775–2780. https://doi.org/10.1007/s11581-016-1901-0

32. Arockia Mary I, Selvanayagam S, Selvasekarapandian S, Srikumar SR, Ponraj T, Moniha V (2019) Lithium ion conducting membrane based on K-carrageenan complexed with lithium bromide and its electrochemical applications. Ionics (Kiel) 25:5839–5855. https://doi.org/10.1007/s11581-019-03150-x

33. Cholant CM, Rodrigues MP, Peres LL, Balboni RDC, Krüger LU, Placido DN, Flores WH, Gündel A, Pawlicka A, Avellaneda CO (2020) Study of the conductivity of solid polymeric electrolyte based on PVA/GA blend with addition of acetic acid. J Solid State Electrochem 24:1867–1875. https://doi.org/10.1007/s10008-020-04605-2

34. Sangeetha P, Selvakumari TM, Selvasekarapandian S, Srikumar SR, Manjuladevi R, Mahalakshmi M (2020) Preparation and characterization of biopolymer K-carrageenan with MgCl2 and its application to electrochemical devices. Ionics (Kiel) 26:233–244. https://doi.org/10.1007/s11581-019-03193-0

35. KUMAR RK, ANJI REDDY POLU (2011) Impedance spectroscopy and FTIR Studies of PEG—based polymer electrolytes. E-J Chem 8:347–353

36. Mary IA, Selvanayagam S, Selvasekarapandian S, Chitra R, Vengadesh Krishna M, Monisha S (2022) Lithium ion conducting biopolymer membrane based on kappa carrageenan with LiCl and its application to electrochemical devices. Mater Today Proc 58:855–861. https://doi.org/10.1016/j.matpr.2021.10.045

37. Moniha V, Alagar M, Selvasekarapandian S, Sundaresan B, Boopathi G (2018) Conductive bio-polymer electrolyte iota-carrageenan with ammonium nitrate for application in electrochemical devices. J Non Cryst Solids 481:424–434. https://doi.org/10.1016/j.jnoncrysol.2017.11.027

38. Farhana NK, Omar FS, Shanti R, Mahipal YK, Ramesh S, Ramesh K (2019) Iota-carrageenan-based polymer electrolyte: impact on ionic conductivity with incorporation of AmNTFSI ionic liquid for supercapacitor. Ionics (Kiel) 25:3321–3329. https://doi.org/10.1007/s11581-019-02865-1

39. Chimie D (2089) Dynamic study on the mechanism of gelation of carrageenans by ATR-FTIR spectroscopy at variable temperature., (n.d.) 348–349

40. Hirankumar G, Selvasekarapandian S, Bhuvaneswari MS, Baskaran R, Vijayakumar M (2004) AC impedance studies on proton conducting polymer electrolyte complexes (PVA + CH$_3$COONH$_4$). Ionics (Kiel) 10:135–138. https://doi.org/10.1007/BF02410322

41. Aziz SB, Hamsan MH, Kadir MFZ, Karim WO, Abdullah RM (2019) Development of polymer blend electrolyte membranes based on chitosan: dextran with high ion transport properties for EDLC application. Int J Mol Sci. https://doi.org/10.3390/ijms20133369

42. Aziz SB, Hamsan MH, Nofal MM, Karim WO, Brevik I, Brza MA, Abdulwahid RT, Al-Zangana S, Kadir MFZ (2020) Structural, impedance and electrochemical characteristics of electrical double layer capacitor devices based on chitosan: dextran biopolymer blend electrolytes. Polymers (Basel). https://doi.org/10.3390/polym12061411

43. Jothi MA, Vanitha D, Bahadur SA, Nallamuthu N (2021) Investigations of biodegradable polymer blend electrolytes based on cornstarch: PVP: NH4Cl and its potential application in solid-state batteries. J Mater Sci Mater Electron 32:5427–5441. https://doi.org/10.1007/s10854-021-05266-1

44. Nandhinilakshmi M, Vanitha D (2022) Dielectric relaxation behaviour and ionic conductivity for corn starch and PVP with sodium fluoride. J Mater Sci Mater Electron 33:12648–12662. https://doi.org/10.1007/s10854-022-08214-9

45. Vanitha D, Bahadur SA, Nallamuthu N, Shunmuganarayanan A, Manikandan A (2017) Studies on conducting polymer blends: synthesis and characterizations of PVA/PVP Doped with CaCl 2. J Nanosci Nanotechnol 18:1723–1729. https://doi.org/10.1166/jnn.2018.14215

46. Abarna S, Hirankumar G (2019) Vibrational, electrical, dielectric and optical properties of PVA-LiPF6 solid polymer electrolytes. Mater Sci Pol 37:331–337. https://doi.org/10.2478/msp-2019-0037

47. Sundaramahalingam K, Jayanthi S, Vanitha D, Nallamuthu N (2021) Dielectric studies of designed novel sodium-based polymer electrolyte with the effect of adding amino acid. Ionics (Kiel) 27:3919–3932. https://doi.org/10.1007/s11581-021-04116-8

48. Hemalatha R, Alagar M, Selvasekarapandian S, Sundaresan B, Moniha V, Boopathi G, Selvin PC (2019) Preparation and characterization of proton-conducting polymer electrolyte based on PVA, amino acid proline, and NH 4 cl and its applications to electrochemical devices. Ionics (Kiel) 25:141–154. https://doi.org/10.1007/s11581-018-2564-9

49. Ahmed HT, Abdullah OG (2020) Structural and ionic conductivity characterization of PEO:MC-NH4I proton-conducting polymer blend electrolytes based films. Results Phys 16:102861. https://doi.org/10.1016/j.rinp.2019.102861

50. Vieira DF, Avellaneda CO, Pawlicka A (2007) Conductivity study of a gelatin-based polymer electrolyte. Electrochim Acta 53:1404–1408. https://doi.org/10.1016/j.electacta.2007.04.034

51. Saroj AL, Singh RK (2012) Journal of physics and chemistry of solids thermal, dielectric and conductivity studies on PVA/ionic liquid [EMIM][EtSO 4] based polymer electrolytes. J Phys Chem Solids 73:162–168. https://doi.org/10.1016/j.jpcs.2011.11.012

52. Salleh NS, Aziz SB, Aspanut Z, Kadir MFZ (2016) Electrical impedance and conduction mechanism analysis of biopolymer electrolytes based on methyl cellulose doped with ammonium iodide. Ionics (Kiel) 22:2157–2167. https://doi.org/10.1007/s11581-016-1731-0

53. Moualhi Y, Nofal MM, M'nassri R, Rahmouni H, Selmi A, Gassoumi M, Khirouni K, Cheikrouhou A (2020) Double Jonscher response and contribution of multiple mechanisms in electrical conductivity processes of Fe–PrCaMnO ceramic. Ceram Int 46:1601–1608. https://doi.org/10.1016/j.ceramint.2019.09.131

54. Majid SR, Arof AK (2007) Electrical behavior of proton-conducting chitosan-phosphoric acid-based electrolytes. Phys B Condens Matter 390:209–215. https://doi.org/10.1016/j.physb.2006.08.038

55. Jothi MA, Vanitha D, Bahadur SA, Nallamuthu N (2021) Proton conducting polymer electrolyte based on cornstarch, PVP, and NH4Br for energy storage applications. Ionics (Kiel) 27:225–237. https://doi.org/10.1007/s11581-020-03792-2

56. Yusof YM, Illias HA, Kadir MFZ (2014) Incorporation of NH4Br in PVA-chitosan blend-based polymer electrolyte and its effect on the conductivity and other electrical properties. Ionics (Kiel) 20:1235–1245. https://doi.org/10.1007/s11581-014-1096-1

57. Arya A, Sharma AL (2018) Effect of salt concentration on dielectric properties of Li-ion conducting blend polymer electrolytes. J Mater Sci Mater Electron 29:17903–17920. https://doi.org/10.1007/s10854-018-9905-3

58. Singh KP, Gupta PN (1998) Study of dielectric relaxation in polymer electrolytes. Eur Polym J 34:1023–1029. https://doi.org/10.1016/S0014-3057(97)00207-3

59. Duraikkan V, Sultan AB, Nallaperumal N, Shunmuganarayanan A (2018) Structural, thermal and electrical properties of polyvinyl alcohol/poly(vinyl pyrrolidone)–sodium nitrate solid polymer blend electrolyte. Ionics (Kiel) 24:139–151. https://doi.org/10.1007/s11581-017-2169-8

60. Jayanthi S, Sundaresan B (2014) Effect of ultrasonic irradiation and TiO 2 on the determination of electrical and dielectric properties of PEO–P (VdF–HFP)–LiClO 4 -based nanocomposite polymer blend electrolytes. Ionics (Kiel). https://doi.org/10.1007/s11581-014-1230-0

61. Aziz SB, Karim WO, Brza MA, Abdulwahid RT, Saeed SR, Al-Zangana S, Kadir MFZ (2019) Ion transport study in CS: POZ based polymer membrane electrolytes using Trukhan model. Int J Mol Sci 20:1–20. https://doi.org/10.3390/ijms20215265

62. Asnawi ASFM, Aziz SB, Brevik I, Brza MA, Yusof YM, Alshehri SM, Ahamad T, Kadir MFZ (2021) The study of plasticized sodium ion conducting polymer blend electrolyte membranes based on chitosan/dextran biopolymers: ion transport, structural, morphological and potential stability. Polymers (Basel) 13:1–25. https://doi.org/10.3390/polym13030383

63. Aziz SB, Gh O, Ahang A (2017) Electrolytes: two methods for band gap study optical properties of pure and doped PVA: PEO based solid polymer blend electrolytes: two methods for band gap study. J Mater Sci Mater Electron. https://doi.org/10.1007/s10854-017-6437-1

64. Irfan M, Manjunath A, Mahesh SS, Somashekar R, Demappa T (2021) Influence of NaF salt doping on electrical and optical properties of PVA/PVP polymer blend electrolyte films for battery application. J Mater Sci Mater Electron 32:5520–5537. https://doi.org/10.1007/s10854-021-05274-1

65. Aziz SB, Brza MA, Nofal MM, Abdulwahid RT, Hussen SA, Hussein AM, Karim WO (2020) A comprehensive review on optical properties of polymer electrolytes and composites. Materials (Basel). https://doi.org/10.3390/MA13173675

66. Gnana Kiran M, Krishna Jyothi N, Samatha K, Rao MP, Vijayakumar K (2020) Optical properties of TSP: NaNO3 biopolymer electrolyte. Res J Chem Environ 24:27–35

67. Bhavsar V, Tripathi D (2016) Study of refractive index dispersion and optical conductivity of PPy doped PVC films. Indian J Pure Appl Phys 54:105–110

68. Al-Gunaid MQA, G. H.M STE, Al-Ostoot FH, Basavarajaiah S (2020) Optimized nano-perovskite lanthanum cuprate decorated PVA based solid polymer electrolyte. Polym Technol Mater 59:215–229. https://doi.org/10.1080/25740881.2019.1634729

69. Wadatkar NS, Waghuley SA (2015) Complex optical studies on conducting polyindole as-synthesized through chemical route. Egypt J Basic Appl Sci 2:19–24. https://doi.org/10.1016/j.ejbas.2014.12.006

70. Aziz SB, Hassan AQ, Mohammed SJ, Karim WO, Kadir MFZ, Tajuddin HA, Chan NNMY (2019) Structural and optical characteristics of pva:C-dot composites: tuning the absorption of ultra violet (uv) region. Nanomaterials 9:216. https://doi.org/10.3390/nano9020216

71. Arasakumari M (2021) Effect of Anhydrous Gdcl3 Doping on the Structural, Optical and Electrical Properties of PVP Polymer Electrolyte Films,

72. Shanmuga Priya S, Karthika M, Selvasekarapandian S, Manjuladevi R (2018) Preparation and characterization of polymer electrolyte based on biopolymer I-Carrageenan with magnesium nitrate. Solid State Ionics 327:136–149. https://doi.org/10.1016/j.ssi.2018.10.031

73. Aziz SB, Hamsan MH, Abdullah RM, Abdulwahid RT, Brza MA, Marif AS, Kadir MFZ (2020) Protonic EDLC cell based on chitosan (CS): methylcellulose (MC) solid polymer blend electrolytes. Ionics (Kiel) 26:1829–1840. https://doi.org/10.1007/s11581-020-03498-5

74. Nallamuthu N, Manikandan M, Jothi AAnandha, Vanitha D, Asath Bahadur S (2020) Investigations of lithium ion conducting polymer blend electrolytes using biodegradable cornstarch and PVP. Phys B Condens Matter 580:411940. https://doi.org/10.1016/j.physb.2019.411940

75. Selvasekarapandian S, Baskaran R, Hema M (2005) Complex AC impedance, transference number and vibrational spectroscopy studies of proton conducting PVAc – NH 4 SCN polymer electrolytes. Phy B: Condens Matter 357:412–419. https://doi.org/10.1016/j.physb.2004.12.007

76. Dannoun EMA, Aziz SB, Abdullah SN, Nofal MM, Mahmoud KH, Murad AR, Abdullah RM, Kadir MFZ (2021) Characteristics of Plasticized Lithium Ion conducting Green Polymer Blend Electrolytes based on CS: Dextran with High Energy Density and specific capacitance, 1–19

77. Qiu Y, Fan H, Chang X, Dang H, Luo Q, Cheng Z, Arunpandiyan S, Raja A, Bharathi S, Arivarasan A, Subagio A, Al Hakim Y, Ristiawan MW, Kholil MA, Priyono S, Arunpandiyan S, Vinoth A, Pandikumar A, Raja A, Arivarasan S, Vinoth A, Pandikumar A, Arivarasan GH, Gote M, Pathak MA, More DJ, Late CS, Rout M, Isacfranklin C, Deepika G, Ravi R, Yuvakkumar D, Velauthapillai B, Saravanakumar R, Packiaraj KS, Venkatesh P, Devendran SA, Bahadur N, Nallamuthu C, Wu L, Shen Q, Huang YC, Zhang S, Balachandran M, Swaminathan L, Li X, Zhang Z, Zhang M, Zhang L, Cong Y, Pan S, Lin X, Yu J, Sun W, Zhao S, Zhao H, Chen K, Tao Y, Hu L, Han Y, Huang L, Quan T, Liu Q, Chen D, Cai H, Zhan M, Zirak M, Azinfar M, Khalili S, Ansari MS, Ansari SP, Satsangee R, Jain S, Ezhil Arasi P, Devendran R, Ranjithkumar S, Arunpandiyan A, Arivarasan AM, Abdulkarem AA, Aref A, Abdulhabeeb YF, Li Y, Yu TP, Gujar VR, Shinde CD, Lokhande SH, Han S, Veeralakshmi S, Kalaiselvam R, Murugan P, Pandurangan S, Nehru S, Sakthinathan TW, Chiu (2020) Development of pristine and Au-decorated Bi2O3/Bi2WO6 nanocomposites for supercapacitor electrodes. Mater Sci Semicond Process 106:32573–32580. https://doi.org/10.1039/c9ra06112f

78. Aziz SB, Dannoun EMA, Abdulwahid RT, Kadir MFZ, Nofal MM, Al-Saeedi SI, Murad AR (2022) The study of ion transport parameters in MC-based electrolyte membranes using EIS and their applications for EDLC devices. Membranes (Basel). https://doi.org/10.3390/membranes12020139

79. Aziz SB, Nofal MM, Kadir MFZ, Dannoun EMA, Brza MA, Hadi JM, Abdullah RM (2021) Bio-based plasticized PVA based polymer blend electrolytes and electrochemical properties. Materials (Basel) 14:1994